VIBRATION LOCALIZATION AND WAVE CONVERSION PHENOMENA IN A MULTI-COUPLED, NEARLY PERIODIC, DISORDERED TRUSS BEAM *

Wan Joe Chen†
Christophe Pierre‡
Department of Mechanical Engineering and Applied Mechanics
The University of Michigan
Ann Arbor, Michigan

0. ABSTRACT

An investigation of the free dynamics of nearly periodic disordered truss beams is presented. An *exact wave transfer matrix* methodology is chosen in order to examine the effects of slight disorder among the bays upon the propagation of waves and the transmission of vibration through the truss beam. It is shown that both free harmonic waves and modes of vibration that extend throughout the entire ordered structure may become *localized* to a few of the bays of the disordered truss beam. In order to examine the interactions among the various waves present in the structure, the concept of power flow is utilized as a scalar descriptor of localization. The mechanism of localization for this multi-coupled system is much richer and more complex than for mono-coupled systems. Specifically, the leakage of energy from the wave pair that is most subject to localization to wave pairs that are less prone to localization is observed, suggesting that localization is more difficult to achieve in multi-coupled systems than in mono-coupled ones. Also, localization occurs primarily at higher frequencies, when individual structural members resonate. It does not occur for global bending vibration modes. These are believed to be the first results on localization for multi-coupled nearly periodic structures. The wave conversion mechanism evidenced here is a novel phenomenon that is probably characteristic of disorder effects in multi-coupled structures.

1. INTRODUCTION

The individual bays that make up a spatially periodic engineering structure, such as a truss beam, are never exactly identical, because perfect periodicity is prevented by unavoidable manufacturing tolerances and other defects. These periodicity-destroying irregularities are referred to as mistuning, or disorder. It is now well-known that, under certain conditions of weak internal coupling, or equivalently, of high modal density, small disorder among the bays of a periodic structure leads to the qualitative alteration of its dynamics, by *localizing* the mode shapes of vibration to small geometric regions and by trapping the free harmonic waves near the energy source. We refer the reader to the work of Pierre,[1] Hodges,[2] and Bendiksen[3] for fundamental studies of wave and mode localization phenomena.

The mechanism of mode localization in nearly periodic structures is well understood, at least for the simple class of mono-coupled structures (see Pierre,[1] Hodges,[2] Bendiksen,[3] and Kissel[4]). Mono-coupled structures are characterized by a single coupling coordinate between two adjacent bays, and thus feature a single pair of left- and right-traveling waves. When one wave impinges on a different medium (for example, at the junction of two slightly different bays), part of it is reflected and part is transmitted. It is these multiple reflections at the junctions between the random bays that cause the localization of incident waves. The mechanism for localization is thus one of energy re-distribution, not one of energy dissipation, such that the energy remains confined to a small geometric region. This results in larger vibration amplitudes locally and hence in reduced fatigue life, for example for turbomachinery rotors. On the other hand, the localization of propagating disturbances near the excitation source may have useful passive control applications for space structures such as truss beams.

Periodic truss beams are doubtlessly subject to periodicity-destroying irregularities, because of discrepancies either among the properties (*e.g.* the length) of individual structural members or among the characteristics of the numerous joints that link structural members (*e.g.*, imperfect fits, clearances, and in-service degradation). Also, previous studies have shown that truss beams may possess very closely-spaced modes and thus high modal densities.[5] Therefore, it is likely that, at least in the frequency ranges that feature local vibrations of the truss members, the dynamics of truss beams is highly sensitive to such irregularities and that localization occurs. Truss beams, however, are *multi-coupled* periodic structures (*i.e.*, the bays are coupled through more than one coordinate) and the theory of localization for multi-coupled structures is not well developed yet. This may explain why there have not been any studies of the localization phenomenon in truss beams, except for the localized normal modes reported in the work of Friedmann *et al.*,[6] who used a finite element approach.

The main reason no general theory of localization is yet available for multi-coupled disordered structures is that these systems feature a much more complicated wave propagation mechanism than mono-coupled ones, due to the existence of more than one type of characteristic waves in the periodic structure. In particular, if a wave of a given type impinges on the junction of two random bays, it produces not only a reflected and a transmitted component of the same type as the incident wave, but also transmitted and reflected components of all the other types of characteristic waves present in the structure. This leakage of energy into other wave types is what makes the study of localization for multi-coupled systems more challenging, as well as more interesting, than for mono-coupled structures. Although there is a dearth of research on multi-coupled localization, we point out to the promising recent development by Kissel,[4] who initiated a general theory that should pave the way for future studies. Also, in a recent study, Igusa and Tang[7] presented an integral form that approximates asymptotically the dynamic response when the modal density is high. These two developments have potential to yield advances in the field of multi-coupled localization, with immediate application to truss beams.

In this paper we examine the occurrence of wave and mode localization in a disordered truss beam with simple geometry. The study is a continuation of the research presented in reference 5, which dealt primarily with the dynamics of ordered truss beams. Here, we adopt the same wave transfer matrix methodology as in reference 5, and a key aspect of the formulation is that the dynamics of one bay is represented by a linearly *exact* transfer matrix. Thus the dynamics of the entire truss beam is simply described by a product of transfer matrices. However, contrary to the case of a periodic truss beam, the methodology faces severe numerical problems for the disordered system when taking the product of random wave transfer matrices. In order to circumvent this difficulty, we develop in this paper a new algorithm to calculate accurately the

* This work is supported by NSF Grant No. MSS-8913196.
† Graduate Research Assistant. Member AIAA.
‡ Associate Professor. Member AIAA, ASME.

wave amplitudes at all bays. This allows us to obtain an accurate depiction of the dynamics even at those (high) frequencies where individual structural members undergo resonances. As a result, we are able to tackle the difficult (both analytically and numerically) problem of localization in truss beams with structural irregularities and to obtain waves and modes with various degrees of localization for different frequencies. A key result is that waves that localize most appear to leak their energy to other waves that feature weaker localization. Hence, in multi-coupled systems, the propagation of wave motion can be sustained by one wave, although the incident wave may become strongly localized. We believe the wave conversion evidenced here is a new mechanism for localization that is characteristic of disordered multi-coupled systems.

Another focus of the paper is the use of power flow as a descriptor of wave localization. Power flow is defined as the time-averaged power (force times velocity) at the junctions between bays; it describes the amount of power which is transmitted by waves through the structure. Mead[9] first introduced the concept of power flow for multi-coupled periodic structures and he showed that only passband waves can transmit energy. Signorelli and von Flotow[10] applied these findings to the characteristic waves in periodic truss beams. However, to date, power flow has only been utilized to examine wave propagation in perfectly periodic structures. In this paper we generalize the definition of power flow to randomly disordered structures and make use of it as a scalar descriptor to examine the occurrence of wave localization. This makes sense since when an incident wave is subject to localization, its vibrational energy is confined to a small geometric region, which implies that only a small amount of power is transmitted along the structure.

The paper is organized as follows. Section 2 describes the exact wave transfer matrix methodology for a general multi-coupled disordered structure. We first set the problem of harmonic waves propagating through a disordered segment and propose an algorithm to resolve the numerical difficulties that arise. We then define the power flow associated with characteristic waves in disordered systems and obtain general results regarding it. Finally, we formulate the eigenvalue problem which governs the modes of vibration of finite structures. In Section 3 we use this formulation to examine the propagation of waves through a disordered two-dimensional truss beam. Wave localization and conversion phenomena are evidenced and studied. In Section 4 we obtain the normal modes of a disordered fixed-fixed truss beam. Finally, Section 5 concludes the paper.

The primary original contributions of the paper lie (1) in the evidence of localization for a multi-coupled disordered structure, (2) in the illustration of the interactions between various wave types in disordered structures, *i.e.*, in the wave conversion phenomenon, (3) in the use of power flow as a descriptor of localization and (4), in the development of an algorithm for predicting the dynamics of large-scale disordered multi-coupled structures.

2. WAVE TRANSFER MATRIX FORMULATION FOR DISORDERED MULTI-COUPLED STRUCTURES

In the wave transfer matrix approach the motion of the structure is regarded as being made of a combination of waves traveling through the structure. This methodology is described in detail in reference 5 for ordered multi-coupled structures, in which case the waves that make up the motion are independent. In this section the wave approach is extended to the case of disordered bays for a general multi-coupled periodic structure and the concept of power flow is introduced. Only the main steps of the formulation are given in Section 2.1, since much of the derivation is similar to that in reference 5.

2.1 METHODOLOGY

Our goal is to study the propagation of a characteristic wave traveling through disordered bays. To that end, we consider the free vibrations of the generic, multi-coupled, nearly periodic structure shown in Fig. 1. This infinite structure consists of a finite segment of N randomly disordered bays embedded in an otherwise ordered structure. We index the disordered bays from 1 to N. All bays for $n = -\infty, \cdots, 0$ and $n = N+1, \cdots, +\infty$ are ordered and thus identical. The bays for $n = 1, \cdots, N$ are randomly disordered and hence slightly different. We restrict the internal coupling in the structure to that between adjacent bays.

Figure 1 depicts one bay, with the independent generalized coordinates through which inter-bay coupling occurs. Let us denote by m the number of coupling coordinates between two bays and by $(\mathbf{U}_n)_L$ and $(\mathbf{F}_n)_L$ the vectors (or the columns) of time-dependent generalized coupling coordinates and generalized forces at the junction of the nth and $(n-1)$th bay. Similarly, denote by $(\mathbf{U}_n)_R$ and $(\mathbf{F}_n)_R$ the time-dependent coupling coordinates and forces at the right end of the nth bay. In general, these vectors describe linear and rotational motions, and each has dimension m. Assuming a single-harmonic motion gives the following equations:

$$(\mathbf{F}_n)_L = (\mathbf{f}_n)_L e^{j\omega t} \tag{1}$$

$$(\mathbf{U}_n)_L = \mathbf{u}_n e^{j\omega t} = (\mathbf{u}_{nR} + j\mathbf{u}_{nI}) e^{j\omega t} \tag{2}$$

where we define $\mathbf{u}_n \equiv (\mathbf{u}_n)_L$ and $j = \sqrt{-1}$, and where $\mathbf{u}_{nR}$ and $\mathbf{u}_{nI}$ are the real and imaginary parts of $\mathbf{u}_n$, respectively. Writing the strain and kinetic energies for a bay in terms of the coupling coordinates, we can derive a frequency-dependent dynamic matrix that relates the force and displacement amplitudes at both ends of a bay. This $2m$ by $2m$ matrix is given by (see Chen and Pierre[5] for detail).

$$\begin{bmatrix} (\mathbf{f}_n)_L \\ (\mathbf{f}_n)_R \end{bmatrix} = (\mathbf{K}_n - \omega^2 \mathbf{M}_n) \begin{bmatrix} \mathbf{u}_n \\ \mathbf{u}_{n+1} \end{bmatrix} = \begin{bmatrix} \mathbf{A}_n & \mathbf{B}_n \\ \mathbf{C}_n & \mathbf{D}_n \end{bmatrix} \begin{bmatrix} \mathbf{u}_n \\ \mathbf{u}_{n+1} \end{bmatrix} \tag{3}$$

where in general the mass and stiffness matrices are symmetric, thus $\mathbf{A}_n = \mathbf{A}_n^T$, $\mathbf{D}_n = \mathbf{D}_n^T$, and $\mathbf{C}_n = \mathbf{B}_n^T$.

The first step of the wave methodology is the formulation of transfer matrices that relate the dynamics at two adjacent bays. These matrices can be defined because we consider only nearest-neighbor coupling. The general form of the transfer matrix is derived in Chen and Pierre[5] for a multi-coupled system and we refer the reader to it for details. Here we choose to define the state at the nth bay by the displacement state vector $\mathbf{x}_n = [\mathbf{u}_n^T, \mathbf{u}_{n-1}^T]^T$, where T denotes a transpose and $\mathbf{u}_n$ is the vector of coupling coordinate amplitudes at the junction of the $(n-1)$th and nth bays. This yields the general form of the displacement transfer matrix:

$$\mathbf{x}_{n+1} = \mathbf{T}_n \mathbf{x}_n = \begin{bmatrix} \mathbf{T}_{1n} & \mathbf{T}_{2n} \\ \mathbf{I} & \mathbf{0} \end{bmatrix} \mathbf{x}_n \tag{4}$$

where

$$\begin{cases} \mathbf{T}_{1n} = -\mathbf{B}_n^{-1}(\mathbf{A}_n + \mathbf{D}_{n-1}) \\ \mathbf{T}_{2n} = -\mathbf{B}_n^{-1}\mathbf{C}_{n-1} \end{cases}$$

Since the number of coupling coordinates between bays is m, $\mathbf{x}_n$ is a $2m$-vector and $\mathbf{T}_{1n}$ and $\mathbf{T}_{2n}$ are m by m matrices. From Eq. (4), the transfer matrix $\mathbf{T}_n$ is determined by the structural properties of the $(n-1)$th bay and those of the nth bay. Hence, for the randomly disordered system shown in Fig. 1, the transfer matrices $\mathbf{T}_n$, for $n = 1, ..., N+1$, are random and generally different from the ordered (or nominal) transfer matrix, which we denote by $\mathbf{T}_o$. Note that the transfer matrix of the $(N+1)$th bay is also random, although that bay is not disordered.

The next step in the wave formulation is to define a coordinate transformation between the displacement and the wave coordinates. To achieve this, we seek characteristic wave motions such that when a wave travels across the junction between two ordered

bays, the state vector is multiplied by a constant. This complex constant accounts for the change in wave amplitude or phase, or both, at the coupling junction. It can be shown easily that characteristic waves are obtained by solving the eigenvalue problem for the transfer matrix $\mathbf{T}_o$ of an *ordered* bay. The constants that characterize the propagating or attenuating nature of the waves are given by the eigenvalues of $\mathbf{T}_o$, while the characteristic wave shapes (the deflection pattern of the structure) are given by the eigenvectors of $\mathbf{T}_o$. The eigenvalues of $\mathbf{T}_o$ occur in reciprocal pairs, hence there are m pairs of left- and right-traveling waves. We can form the matrix $\mathbf{X}$ whose columns are the eigenvectors of $\mathbf{T}_o$, such that the first m columns of $\mathbf{X}$ correspond to the left-traveling waves and the last m columns to right-traveling waves. This allows us to separate left- and right-traveling waves.

The physical displacement amplitude coordinates are then transformed into *wave amplitude coordinates* by a linear transformation that is defined by the matrix of eigenvectors of the *ordered* transfer matrix, $\mathbf{X}$. For the nth bay, we obtain

$$\begin{bmatrix} \mathbf{u}_n \\ \mathbf{u}_{n-1} \end{bmatrix} = \mathbf{X} \begin{bmatrix} \mathbf{L}_n \\ \mathbf{R}_n \end{bmatrix} = \begin{bmatrix} \mathbf{X}_{11} & \mathbf{X}_{12} \\ \mathbf{X}_{21} & \mathbf{X}_{22} \end{bmatrix} \begin{bmatrix} \mathbf{L}_n \\ \mathbf{R}_n \end{bmatrix} \tag{5}$$

where the m-vector $\mathbf{L}_n$ contains the complex amplitudes of the left-traveling waves and the m-vector $\mathbf{R}_n$ those of the right-traveling waves. As shown in Fig. 2, the waves entering the nth bay are $\mathbf{R}_n$ and $\mathbf{L}_{n+1}$ and those leaving the bay are $\mathbf{R}_{n+1}$ and $\mathbf{L}_n$. Each wave coordinate represents the contribution of the corresponding wave to the overall motion. Through the coordinate transformation in Eq. (5), the total motion can be expressed as a linear combination of the characteristic waves. Note that the coordinate transformation takes the same form for ordered and disordered systems. Substituting Eq. (5) into Eq. (4), the wave amplitudes at two adjacent bays are related by

$$\begin{bmatrix} \mathbf{L}_{n+1} \\ \mathbf{R}_{n+1} \end{bmatrix} = \mathbf{X}^{-1}\mathbf{T}_n\mathbf{X} \begin{bmatrix} \mathbf{L}_n \\ \mathbf{R}_n \end{bmatrix} = \mathbf{W}_n \begin{bmatrix} \mathbf{L}_n \\ \mathbf{R}_n \end{bmatrix} \tag{6}$$

where $\mathbf{W}_n$ is the *wave transfer matrix* for the nth bay. At this point it is appropriate to distinguish between ordered and disordered bays.

• For an ordered bay ($-\infty < n \leq 0$ and $N+1 < n < +\infty$)

Then $\mathbf{T}_n \equiv \mathbf{T}_o$ and $\mathbf{W}_n \equiv \mathbf{W}_o = \mathbf{X}^{-1}\mathbf{T}_o\mathbf{X}$. Since $\mathbf{X}$ is the matrix of eigenvectors of $\mathbf{T}_o$, the wave transfer matrix is the diagonal matrix of the eigenvalues of $\mathbf{T}_o$. It has the form:

$$\mathbf{W}_o = \begin{bmatrix} \mathbf{\Lambda} & \mathbf{0} \\ \mathbf{0} & \mathbf{\Lambda}^{-1} \end{bmatrix} \tag{7}$$

where $\mathbf{\Lambda}$ is a diagonal matrix representing the left-traveling waves (its elements have modulus greater than or equal to one) and $\mathbf{\Lambda}^{-1}$ corresponds to the reciprocal right-traveling waves. Equations (6) and (7) tell us that the $2m$ characteristic components of a wave incident to the junction of two ordered bays are not only fully transmitted through the junction and not reflected, but also remain independent and do not exchange energy with one another. This means that in an ordered structure characteristic waves travel independently.

• For a disordered bay ($0 < n \leq N+1$)

The wave transfer matrix for the nth disordered bay, $\mathbf{W}_n$, is no longer a diagonal matrix, because the transformation defined by $\mathbf{X}$ does not diagonalize the random transfer matrix $\mathbf{T}_n$. This allows for scattering at the junction of two disordered bays as well as for exchange of energy among the various types of characteristic waves, through both reflections and transmissions of one wave type into the other types.

Using the recursive form of Eq. (6), we can relate the wave amplitudes at both ends of the disordered segment, that is, those at site 1 to those at site $(N+2)$, as

$$\begin{bmatrix} \mathbf{L}_{N+2} \\ \mathbf{R}_{N+2} \end{bmatrix} = (\mathbf{W}_{N+1}...\mathbf{W}_1) \begin{bmatrix} \mathbf{L}_1 \\ \mathbf{R}_1 \end{bmatrix} = \begin{bmatrix} \mathbf{\Theta} & \mathbf{\Phi} \\ \mathbf{\Gamma} & \mathbf{\Psi} \end{bmatrix} \begin{bmatrix} \mathbf{L}_1 \\ \mathbf{R}_1 \end{bmatrix} \tag{8}$$

Since our primary interest lies in the localization of waves traveling through disordered bays, we choose to examine the propagation of a characteristic wave that is incident from the left to bay 1 and is represented by the wave amplitude vector $\mathbf{R}_1$. If there were no disordered bays in the infinite structure, this wave would be fully transmitted without encountering any reflection nor any alterations. Specifically, the m right-traveling characteristic components of the wave (represented by $\mathbf{R}_1$) would remain independent and not exchange energy with other characteristic waves as they travel through the structure. Mathematically, this means that we would have $\mathbf{L}_{N+2} = \mathbf{L}_1 = \mathbf{0}$ and $\mathbf{R}_{N+2} = \mathbf{\Lambda}^{-(N+1)}\mathbf{R}_1$, with $\mathbf{\Lambda}$ diagonal. However, when we send the same incident wave through the disordered segment, there are not only reflections for each type of waves, but also exchanges of energy between the various types of (transmitted and reflected) characteristic waves at each junction between disordered bays. This means that the reflected wave amplitudes $\mathbf{L}_1$ through $\mathbf{L}_{N+1}$ are different from zero. Moreover, we have $\mathbf{L}_{N+2} = \mathbf{L}_{N+3} = ... = \mathbf{0}$, since all bays to the right of the disordered segment are ordered and thus do not cause reflections. Using the facts that $\mathbf{L}_{N+2} = \mathbf{0}$ and $\mathbf{R}_1$ is a known vector, we can solve for $\mathbf{L}_1$ in terms of $\mathbf{R}_1$ from Eq. (8). We obtain:

$$\mathbf{L}_1 = -\mathbf{\Theta}^{-1}\mathbf{\Phi}\mathbf{R}_1 \tag{9}$$

Once $\mathbf{L}_1$ is determined, we can calculate the wave amplitudes at all bays from Eq. (6), simply by multiplying by the appropriate disordered wave transfer matrices. In particular, the vector of wave amplitudes transmitted through the disordered segment, a quantity of special interest in localization studies, is given by:

$$\mathbf{R}_{N+2} = \mathbf{\Gamma}\mathbf{L}_1 + \mathbf{\Psi}\mathbf{R}_1 \tag{10}$$

Afterwards, the physical displacement vector at each bay is readily obtained from Eq. (5).

The above wave formulation faces severe numerical problems in practice, namely when the displacement transfer matrix has a large eigenvalue (of the order of 1000) and when the number of bays is not small (greater than 10). This is because calculating the amplitudes reflected by the disordered segment, $\mathbf{L}_1$, requires taking the product of the nearly diagonal wave transfer matrices that characterize the disordered bays. Multiplying these matrices generates significant errors when some diagonal elements of $\mathbf{W}_n$ (corresponding to the large eigenvalues of $\mathbf{T}_o$) are large compared to off-diagonal elements. This occurs because the errors present in the small off-diagonal terms (which themselves are due to inaccuracies in $\mathbf{X}$ and its inverse) are amplified by the large diagonal elements at each wave transfer matrix multiplication. It results in an incorrect wave amplitude $\mathbf{L}_1$, which means that all other wave amplitudes cannot be obtained from Eq. (6). In order to overcome this numerical problem, the following algorithm is developed to calculate accurately the wave amplitudes at all sites.

2.2 AN ALGORITHM FOR WAVE AMPLITUDES IN LARGE DISORDERED STRUCTURES

The motivation for this algorithm is the desire to lessen the magnification of numerical inaccuracy caused by the multiplication of matrices containing large numbers. In order to curb this error, we make use of the fact that $\mathbf{L}_{N+2} = \mathbf{0}$ (recall that all bays to the right of the disordered region are ordered). By expressing $\mathbf{L}_{N+2}$ as a product of wave transfer matrices and the wave amplitude vector at site 1, and then performing appropriate operations on each side of the equation, we can reduce the error due to large numbers in each matrix multiplication.

For convenience, the wave transfer matrix of an arbitrary nth bay is denoted by

$$\mathbf{W}_n = \begin{bmatrix} \Theta_n & \Phi_n \\ \Gamma_n & \Psi_n \end{bmatrix} \tag{11}$$

where all submatrices are m by m and Θ_n contains large numbers on its diagonal (corresponding to left-traveling waves). Using Eqs. (8) and (11), we can express $\mathbf{L}_{N+2}$ as

$$\mathbf{L}_{N+2} = \mathbf{0} = [\,\Theta_{N+1} \quad \Phi_{N+1}\,] \begin{bmatrix} \Theta_N & \Phi_N \\ \Gamma_N & \Psi_N \end{bmatrix} \cdots \begin{bmatrix} \Theta_1 & \Phi_1 \\ \Gamma_1 & \Psi_1 \end{bmatrix} \begin{bmatrix} \mathbf{L}_1 \\ \mathbf{R}_1 \end{bmatrix} \tag{12}$$

In order to reduce the possible error amplified by the large numbers in Θ_{N+1}, we pre-multiply both sides of Eq. (12) by Θ_{N+1}^{-1}. This yields

$$\mathbf{0} = [\,\mathbf{I} \quad \Theta_{N+1}^{-1}\Phi_{N+1}\,] \begin{bmatrix} \Theta_N & \Phi_N \\ \Gamma_N & \Psi_N \end{bmatrix} \cdots \begin{bmatrix} \Theta_1 & \Phi_1 \\ \Gamma_1 & \Psi_1 \end{bmatrix} \begin{bmatrix} \mathbf{L}_1 \\ \mathbf{R}_1 \end{bmatrix} \tag{13}$$

Next, the first product in Eq. (13) is expanded. This yields:

$$\mathbf{0} = [\,\Theta_N + \mathbf{S}_{N+1}\Gamma_N \quad \Phi_N + \mathbf{S}_{N+1}\Psi_N\,] \begin{bmatrix} \Theta_{N-1} & \Phi_{N-1} \\ \Gamma_{N-1} & \Psi_{N-1} \end{bmatrix} \cdots \begin{bmatrix} \Theta_1 & \Phi_1 \\ \Gamma_1 & \Psi_1 \end{bmatrix} \begin{bmatrix} \mathbf{L}_1 \\ \mathbf{R}_1 \end{bmatrix} \tag{14}$$

$$\text{where} \quad \mathbf{S}_{N+1} = \Theta_{N+1}^{-1}\Phi_{N+1} \tag{15}$$

Again, to reduce the possible error amplified by the large numbers in Θ_N, we pre-multiply both sides of Eq. (14) by $(\Theta_N + \mathbf{S}_{N+1}\Gamma_N)^{-1}$. Thus,

$$\mathbf{0} = [\,\mathbf{I} \quad (\Theta_N + \mathbf{S}_{N+1}\Gamma_N)^{-1}(\Phi_N + \mathbf{S}_{N+1}\Psi_N)\,] \begin{bmatrix} \Theta_{N-1} & \Phi_{N-1} \\ \Gamma_{N-1} & \Psi_{N-1} \end{bmatrix} \cdots \begin{bmatrix} \Theta_1 & \Phi_1 \\ \Gamma_1 & \Psi_1 \end{bmatrix} \begin{bmatrix} \mathbf{L}_1 \\ \mathbf{R}_1 \end{bmatrix} \tag{16}$$

Similarly, the first product in Eq. (16) is expanded and a matrix $\mathbf{S}_N$ is introduced. We obtain

$$\mathbf{0} = [\,\Theta_{N-1} + \mathbf{S}_N\Gamma_{N-1} \quad \Phi_{N-1} + \mathbf{S}_N\Psi_{N-1}\,] \begin{bmatrix} \Theta_{N-2} & \Phi_{N-2} \\ \Gamma_{N-2} & \Psi_{N-2} \end{bmatrix} \cdots \begin{bmatrix} \Theta_1 & \Phi_1 \\ \Gamma_1 & \Psi_1 \end{bmatrix} \begin{bmatrix} \mathbf{L}_1 \\ \mathbf{R}_1 \end{bmatrix} \tag{17}$$

$$\text{where} \quad \mathbf{S}_N = (\Theta_N + \mathbf{S}_{N+1}\Gamma_N)^{-1}(\Phi_N + \mathbf{S}_{N+1}\Psi_N) \tag{18}$$

If we repeat recursively N times the procedure described above and at each iteration introduce the proper substitution matrix $\mathbf{S}_n$, we end up with

$$\mathbf{0} = [\,\mathbf{I} \quad \mathbf{S}_2\,] \begin{bmatrix} \Theta_1 & \Phi_1 \\ \Gamma_1 & \Psi_1 \end{bmatrix} \begin{bmatrix} \mathbf{L}_1 \\ \mathbf{R}_1 \end{bmatrix} \tag{19}$$

$$\mathbf{0} = [\,\mathbf{I} \quad \mathbf{S}_1\,] \begin{bmatrix} \mathbf{L}_1 \\ \mathbf{R}_1 \end{bmatrix} \tag{20}$$

in which the errors in the off-diagonal elements of $\mathbf{W}_n$ have not been amplified by the large elements in Θ_n. Since $\mathbf{R}_1$ is a selected right traveling wave amplitude, we can calculate $\mathbf{L}_1$ in term of $\mathbf{R}_1$ from Eq. (20):

$$\mathbf{L}_1 = -\mathbf{S}_1\mathbf{R}_1 \tag{21}$$

Next, we use $\mathbf{L}_1$ and $\mathbf{R}_1$ to calculate $\mathbf{L}_2$ and $\mathbf{R}_2$. From Eq. (6) and (11) we have

$$\begin{bmatrix} \mathbf{L}_2 \\ \mathbf{R}_2 \end{bmatrix} = \begin{bmatrix} \Theta_1 & \Phi_1 \\ \Gamma_1 & \Psi_1 \end{bmatrix} \begin{bmatrix} \mathbf{L}_1 \\ \mathbf{R}_1 \end{bmatrix} \tag{22}$$

Then, Eq. (19) becomes

$$\mathbf{0} = [\,\mathbf{I} \quad \mathbf{S}_2\,] \begin{bmatrix} \mathbf{L}_2 \\ \mathbf{R}_2 \end{bmatrix} \tag{23}$$

We use Eq. (22) to solve for $\mathbf{R}_2$ but not for $\mathbf{L}_2$. This is because large numbers in Θ_1 will again amplify the error while calculating $\mathbf{L}_2$. This error will be carried over and accumulated in the successive calculations of wave amplitudes at other sites. To avoid this, we first use Eq. (22) to solve for $\mathbf{R}_2$ and then bring $\mathbf{R}_2$ into Eq. (23) to solve for $\mathbf{L}_2$, since $\mathbf{S}_2$ has already been calculated. Having determined the wave amplitudes at site 2, we are able to calculate those at site 3, site 4, and so on by repeating the same process as for $\mathbf{R}_2$ and $\mathbf{L}_2$. Therefore, the wave amplitudes at all sites can be obtained accurately using this algorithm.

2.3 POWER FLOW: A DESCRIPTOR OF WAVE LOCALIZATION

We study the power flow associated with waves propagating through undamped, multi-coupled, disordered periodic structures. When a wave propagates, it transmits energy along the structure. Since the internal coupling is restricted to adjacent bays, each bay receives or transmits energy through its two junctions with the neighboring bays. The resulting flow of power that travels through the structure in the direction of the incident wave can be quantified by taking the time-average of the input or output power at each junction. This average power flow, which accounts for the interaction between the various transmitted and reflected waves, indicates how much of the input (incident) power is being conveyed through the structure. Power flow is a function of frequency and of the composition of the incident waves and thus it can be used to define the filtering properties of ordered and disordered periodic structures. This can be of use for passive control applications. Moreover, power flow is a convenient scalar that provides physical insights into the interactions of waves and thus into localization phenomena.

Power flow in perfectly periodic, undamped structures has been studied in references 9 and 10, although their definitions of power differ slightly. Mead was first to show that the power flow associated with a passband wave is identical at all bay junctions, and that the power flow associated with a complexband or a stopband wave is zero (although complexband waves are propagating, the net power flow is zero). Thus power can only be transmitted along periodic structures by passband waves and the power flow is constant throughout the structure.

In this work we adopt the definition of power of Signorelli and von Flotow[10] and extend the definition of power flow to a disordered multi-coupled structure. Referring to Fig. 1, we define the instantaneous input power, $p_n(t)$, at the left-hand junction of the nth bay as

$$p_n(t) = \mathrm{Re}[(\mathbf{F}_n)_L^T]\mathrm{Re}[(\dot{\mathbf{U}}_n)_L] \tag{24}$$

where $\mathrm{Re}[(\mathbf{F}_n)_L]$ is the real part of the coupling force at the junction and $\mathrm{Re}[(\dot{\mathbf{U}}_n)_L]$ the real part of the nodal velocity vector. Note that $p_n(t)$ is a scalar. The power flow P_n is defined as the time average over one period $T = 2\pi/\omega$ of the instantaneous power:

$$P_n = \frac{1}{T}\int_0^T p_n(t)dt \tag{25}$$

The force and velocity amplitudes in Eqs. (1) and (2) are substituted into Eq. (24). Then Eq. (3) is used to express the forces in terms of the nodal displacements. This yields:

$$\begin{aligned}\mathrm{Re}[(\mathbf{F}_n)_L] =& (\mathbf{B}_n\mathbf{u}_{(n+1)R} + \mathbf{A}_n\mathbf{u}_{nR})\cos(\omega t) \\ &- (\mathbf{B}_n\mathbf{u}_{(n+1)I} + \mathbf{A}_n\mathbf{u}_{nI})\sin(\omega t)\end{aligned} \tag{26}$$

$$\mathrm{Re}[(\dot{\mathbf{U}}_n)_L] = -\omega(\mathbf{u}_{nR}\sin(\omega t) + \mathbf{u}_{nI}\cos(\omega t)) \tag{27}$$

Next, we substitute Eqs. (26) and (27) into Eq. (24). Using this expression for $p_n(t)$ and the fact that $\mathbf{B}_n^T = \mathbf{C}_n$, we obtain the power flow in Eq. (25) as:

$$P_n = -\frac{\omega}{2}\mathrm{Im}[\mathbf{u}_{n+1}^{*T}\mathbf{C}_n\mathbf{u}_n] \tag{28}$$

where * denotes a complex conjugate and Im an imaginary part. The power flow P_n is thus determined by the displacement vectors on each side of the nth bay and by the matrix $\mathbf{C}_n$. From Eq. (3), recall that $\mathbf{C}_n$ represents the coupling between two adjacent junctions. It is this coupling which allows for energy conversion among waves and power transmission. Note that the power flow is also an explicit function of frequency.

Using Eq. (28), we can show that for a perfectly periodic, undamped structure the power flow associated with a passband wave is nonzero and identical at all bays, while power flow for a complexband or a stopband wave is zero. These proofs are given in Appendix A.

Next, we derive a general result for power flow in disordered structures. From Eq. (4), we have

$$\mathbf{u}_{n+1} = -\mathbf{B}_n^{-1}(\mathbf{A}_n + \mathbf{D}_{n-1})\mathbf{u}_n - \mathbf{B}_n^{-1}\mathbf{C}_{n-1}\mathbf{u}_{n-1} \tag{29}$$

Multiplying both sides by $-\mathbf{u}_n^{*T}\mathbf{B}_n$ yields

$$-\mathbf{u}_n^{*T}\mathbf{B}_n\mathbf{u}_{n+1} = \mathbf{u}_n^{*T}(\mathbf{A}_n + \mathbf{D}_{n-1})\mathbf{u}_n + \mathbf{u}_n^{*T}\mathbf{C}_{n-1}\mathbf{u}_{n-1} \tag{30}$$

Note that the three terms in Eq. (30) are complex scalars and that $(\mathbf{A}_n + \mathbf{D}_{n-1})$ is symmetric and real, since both $\mathbf{A}_n$ and $\mathbf{D}_{n-1}$ are real symmetric. Therefore, $\mathbf{u}_n^{*T}(\mathbf{A}_n + \mathbf{D}_{n-1})\mathbf{u}_n$ is equal to its conjugate transpose and thus it must be real. Then taking the imaginary part of Eq. (30) yields

$$-\mathrm{Im}[\mathbf{u}_n^{*T}\mathbf{B}_n\mathbf{u}_{n+1}] = \mathrm{Im}[\mathbf{u}_n^{*T}\mathbf{C}_{n-1}\mathbf{u}_{n-1}] \tag{31}$$

Using that $\mathbf{u}_n^{*T}\mathbf{B}_n\mathbf{u}_{n+1}$ equals its transpose and that $\mathbf{B}_n^T = \mathbf{C}_n$, we rewrite Eq. (31) as:

$$-\mathrm{Im}[\mathbf{u}_{n+1}^T\mathbf{C}_n\mathbf{u}_n^*] = \mathrm{Im}[\mathbf{u}_n^{*T}\mathbf{C}_{n-1}\mathbf{u}_{n-1}] \tag{32}$$

Finally, transforming the negative sign on the left-hand side of Eq. (32) into a complex conjugate gives

$$\mathrm{Im}[\mathbf{u}_{n+1}^{*T}\mathbf{C}_n\mathbf{u}_n] = \mathrm{Im}[\mathbf{u}_n^{*T}\mathbf{C}_{n-1}\mathbf{u}_{n-1}] \tag{33}$$

or, from Eq. (28):

$$P_n = P_{n-1} \tag{34}$$

We have shown the important property that all bays transmit the same power to the next bay, *i.e.*, the power flow in an disordered undamped structure is constant along the structure. This means that the result obtained by Mead[9] for the special case of periodic structures holds for disordered systems as well. Note that this result is physically reasonable. Since we consider the free vibration of an undamped structure, the one-cycle power received by any bay must be equal to the output power to the adjacent bay. Otherwise, the energy of a bay could increase until failure occurs, which obviously is not the case. Also note that this result permits the use of a single scalar to describe wave transmission and interactions in a compact and global manner. This suggests power flow as a useful descriptor of wave localization.

Using Eq. (5), we can express P_n in Eq. (28) in terms of wave amplitude coordinates:

$$\begin{aligned} P_n = -\frac{\omega}{2}\mathrm{Im}[&\mathbf{R}_{n+1}^{*T}(\mathbf{X}_{12}^{*T}\mathbf{C}_n\mathbf{X}_{22})\mathbf{R}_{n+1} - \mathbf{L}_{n+1}^{*T}(\mathbf{X}_{21}^{*T}\mathbf{C}_n^T\mathbf{X}_{11})\mathbf{L}_{n+1} \\ &+ \mathbf{R}_{n+1}^{*T}(\mathbf{X}_{12}^{*T}\mathbf{C}_n\mathbf{X}_{21} - \mathbf{X}_{22}^{*T}\mathbf{C}_n^T\mathbf{X}_{11})\mathbf{L}_{n+1}] \end{aligned} \tag{35}$$

This shows that the power flow is composed of three parts: the contribution from transmitted waves, the contribution from reflected waves, and the joint contribution from the interaction of transmitted and reflected waves. Without formal proof, we contend that a wave propagating toward the right should result in a positive power flow. Therefore, a left-traveling wave is expected to transmit negative power flow to the right (*i.e.* positive power flow to the left). Using this argument we explain that the first two terms in the right-hand side of Eq. (35) have opposite signs, which indicates that part of the incident energy is not transmitted through the structure due to wave reflections.

Next we apply Eq. (35) to a selected wave incident from the left and traveling through the disordered structure, as described in Section 2.2. Since $\mathbf{L}_{N+2} = \mathbf{0}$, we choose the site $n = N + 2$ to calculate the power flow in the structure. The power flow P at any site can be simply written as:

$$P = P_{N+2} = -\frac{\omega}{2}\mathrm{Im}[\mathbf{R}_{N+2}^{*T}(\mathbf{X}_{12}^{*T}\mathbf{C}_{N+1}\mathbf{X}_{22})\mathbf{R}_{N+2}] \tag{36}$$

Hence the knowledge of the transmitted wave amplitudes, $\mathbf{R}_{N+2}$, is sufficient to determine how much of the incident power passes through the disordered segment. Qualitatively, this power is proportional to the total energy of the waves when they leave the disordered region. The emergent power flow associated with an incident passband wave will, in general, decrease as the disorder level increases, since the scattering of waves becomes large.

It is interesting to note that for a disordered structure, an incident stopband or complexband wave no longer transmits zero power flow (as is the case in perfectly periodic structures). This is because the periodicity-destroying irregularities cause interactions between the various waves, such that passband waves appear as transmitted or reflected waves. This results in a non-zero power flow in the structure, although it may generally be small.

Finally, another interesting result is that if a passband wave is incident to the above disordered structure and if the power flow is calculated at bay $n = 1$, then the joint contribution term in Eq. (35) (the third term in the right-hand side) vanishes. This means that the resultant power flow is simply the difference of the incident power and the power diverted by the reflected waves at site 1. Note that this argument is not true for a stopband or complexband incident wave. The proof is omitted here due to space limitations.

2.4 NORMAL MODES OF A FINITE DISORDERED STRUCTURE

In this section we apply the transfer matrix formulation to determine the normal modes of vibration of finite disordered structures. In order for a finite (undamped) structure to undergo motion in a normal mode at a given frequency, the linear combination of the characteristic waves traveling along the structure at that frequency must form a standing wave, *i.e.*, all degrees of freedom must vibrate in or out of phase.

We consider an N-bay, multi-coupled, disordered structure with fixed-fixed boundary conditions. The bays are numbered from $n = 1$ to N. Our aim is to derive the eigenvalue problem whose solution determines the natural frequencies and associated mode shapes. This can be achieved easily by writing the relation between the displacement vectors at three adjacent bays. We have, from the first block of m equations in Eq. (4):

$$\mathbf{T}_{2n}\mathbf{u}_{n-1} + \mathbf{T}_{1n}\mathbf{u}_n - \mathbf{u}_{n+1} = \mathbf{0} \tag{37}$$

Letting the bay index n in Eq. (37) go from 2 to N, we obtain the following matrix equation:

$$\begin{bmatrix} \mathbf{T}_{22} & \mathbf{T}_{12} & -\mathbf{I} & \mathbf{0} & \cdots & \cdots & \mathbf{0} \\ \mathbf{0} & \mathbf{T}_{23} & \mathbf{T}_{13} & -\mathbf{I} & \mathbf{0} & \cdots & \mathbf{0} \\ \vdots & \ddots & \ddots & \ddots & \ddots & \ddots & \vdots \\ \mathbf{0} & \cdots & \mathbf{0} & \mathbf{T}_{2(N-1)} & \mathbf{T}_{1(N-1)} & -\mathbf{I} & \mathbf{0} \\ \mathbf{0} & \cdots & \cdots & \mathbf{0} & \mathbf{T}_{2N} & \mathbf{T}_{1N} & -\mathbf{I} \end{bmatrix} \begin{bmatrix} \mathbf{u}_1 \\ \vdots \\ \vdots \\ \vdots \\ \mathbf{u}_{N+1} \end{bmatrix} = \mathbf{0} \tag{38}$$

where the matrix has dimension $m(N-1)$ by $m(N+1)$. Next, we

apply the boundary conditions to Eq. (38). Since $\mathbf{u}_1 = \mathbf{u}_{N+1} = \mathbf{0}$ for fixed ends, we eliminate the first and the last m-block columns in Eq. (38). Thus, the rectangular system of equations (38) reduces to a square system of dimension $m(N-1) \times m(N-1)$:

$$\begin{bmatrix} \mathbf{T}_{12} & -\mathbf{I} & \mathbf{0} & \dots & \dots & \mathbf{0} \\ \mathbf{T}_{23} & \mathbf{T}_{13} & -\mathbf{I} & \mathbf{0} & \dots & \mathbf{0} \\ \mathbf{0} & \ddots & \ddots & \ddots & \ddots & \vdots \\ \vdots & \ddots & \ddots & \ddots & \ddots & \mathbf{0} \\ \mathbf{0} & \dots & \mathbf{0} & \mathbf{T}_{2(N-1)} & \mathbf{T}_{1(N-1)} & -\mathbf{I} \\ \mathbf{0} & \dots & \dots & \mathbf{0} & \mathbf{T}_{2N} & \mathbf{T}_{1N} \end{bmatrix} \begin{bmatrix} \mathbf{u}_2 \\ \vdots \\ \vdots \\ \vdots \\ \mathbf{u}_N \end{bmatrix} = \mathbf{0} \quad (39)$$

In order to obtain a non-trivial solution for the structure's displacement vector $[\mathbf{u}_2^T, \dots, \mathbf{u}_N^T]^T$, the determinant of the matrix in Eq. (39) must equal zero. Those frequencies that render this determinant zero are the natural frequencies of the fixed-fixed structure. The associated eigenvectors $[\mathbf{u}_2^T, \dots, \mathbf{u}_N^T]^T$ define the mode shapes that correspond to the natural frequencies.

3. WAVE PROPAGATION IN DISORDERED TRUSS BEAMS

Here we apply the formulation presented in Section 2 to study wave propagation through the truss beam shown in Fig. 3. One bay of the truss beam is shown in Fig. 4. It consists of four pin-joint, uniform, homogeneous structural members. We refer to the members labeled 1, 2, and 3 in Fig. 4 as the longeron beams, and to the structural member labeled 4 as the diagonal beam. Each bay has two nodal points on each side. Because the members are pinned at the joints, there are only two degrees of freedom at each nodal point, two displacements. Hence the number of coupling coordinates between two adjacent bays is four and the transfer matrix for a bay has dimension eight by eight.

An *exact* bay transfer matrix was derived in Chen and Pierre[5] for the truss beam in Fig. 3. It is based upon exact linear models of bending and axial vibrations for each of the four structural members making up a bay. This derivation and the transfer matrix are not given here and we refer the reader to reference 5 for details.

In this section we essentially consider the disordered version of the ordered truss beam studied in Chen and Pierre.[5] We examine the propagation of a selected wave-type through a finite region of randomly disordered bays embedded in an infinite periodic structure. The disorder among the bays originates from differences in their lengths (where the length of a bay is that of the upper or the lower longeron beam). Except for the length variation, the bay geometry is assumed to be unchanged, *i.e.*, the upper and lower longerons have equal lengths and the length of the diagonal member is determined accordingly. Small random disorder is considered, such that the bay lengths are identically and uniformly distributed independent random variables, whose mean is the nominal bay length and standard deviation is σ. In the following we refer to σ as the disorder level.

Since mono-coupled structures feature a single pair of left- and right-traveling waves, the phenomenon of localization occurs simply through multiple reflections of the incident wave at the random bays. In the multi-coupled truss beam studied here, however, an incident wave which impinges on a random bay gives rise to transmitted and reflected waves of each type present in the structure. This mechanism leads not only to the localization of the incident wave, but also to its conversion into other types of waves via energy leakage. In order to evidence these complex phenomena, we consider two truss beams with different structural member axial rigidities: the truss beam with the high axial rigidity features clear wave localization and little energy leakage, while the one with a 100-fold decrease in axial rigidity exhibits pronounced wave conversion as well as localization.

In both cases we investigate the propagation of waves incident from the left into an infinite truss beam which consists of 200 randomly disordered bays embedded in otherwise ordered bays. We first identify the passband structure of the ordered truss beam and then examine the propagation of waves for various disorder levels and frequencies. At some frequencies the associated ordered system features two pairs of passband waves, which allows us to examine how these waves localize and interact in disordered configurations.

3.1 CASE I: WAVE LOCALIZATION PHENOMENON

In this case of high axial rigidity of the structural members the parameters for the truss beams are: $EI = 5.81482 \times 10^3$ Nm^2 (structural member bending rigidity); $EA = 1.93977 \times 10^7$ N (structural member axial rigidity); $m = 0.75948$ Kg/m (mass per unit length of a structural member); and, for an ordered bay, $l_1 = l_2 = l_3 = 1.397$ m (length of the longerons). All members have identical material properties and their axial rigidity is far greater than their bending rigidity.

3.1.1 Characteristic Waves in the Ordered Truss Beam

Before we explore the dynamics of the disordered truss beam, we must first identify the independent wave pairs that characterize the periodic system. We restrict our investigation to the dimensionless frequency range $[0, \pi^2]$, such that π^2 is the fundamental bending frequency of a pinned-pinned vertical longeron beam. (The dimensionless frequency is defined from the frequency as $\bar{\omega} = \omega(ml_1^4/(EI))^{1/2}$. The bar in $\bar{\omega}$ will be dropped for simplicity.) As described in Section 2.1, the characteristic waves are obtained by solving the eigenvalue problem for the ordered transfer matrix $\mathbf{T}_o$: the propagation constants are given by the logarithm of the eigenvalues and the wave shapes by the eigenvectors. Since the transfer matrix of a bay has dimension 8×8, the truss beam carries four pairs of characteristic waves.

The characteristics of these four wave pairs in terms of frequency have been thoroughly investigated by Chen and Pierre[5] and we refer the reader to it for details. Here, we use the power flow defined in Eq. (28) to verify the frequency regions that define the passbands for the various waves. Figure 5 depicts the power flows associated with four pairs of characteristic waves as a function of frequency. Each curve in Fig. 5 is obtained by considering a characteristic wave of unit amplitude incident from the left to the periodic truss beam, and by calculating the corresponding power flow using Eq. (28). Since scattering cannot occur, the transmitted power flow, which is independent of the number of bays, is solely carried by the incident wave. The wave pairs labeled I, II, and III are respectively bending, shear, and compression waves at low frequencies (say $\omega < 4$). In the frequency range shown, the wave pair labeled IV belongs to a stopband and features a very large exponential decay constant (the real part of its propagation constant[5,9]); thus its power flow is zero. For each curve in the figure, regions defined by a non-zero power flow are passbands. Thus for $0 < \omega \leq 4.9318$, the type-I and -III waves are in passbands; for $4.9318 < \omega \leq 5.9115$, only the type-III wave is in a passband; for $5.9115 < \omega \leq 9.8246$, type-II and -III waves are in passbands; for $9.8246 < \omega \leq 9.8584$, type-I, -II, and -III waves are in passbands; and for $9.8584 < \omega \leq \pi^2$, type-I and -II waves are in passbands. Recall that all frequencies are dimensionless.

In general, the power flows depicted in Fig. 5 describe (at least qualitatively) the energy levels associated with the various passband waves of unit amplitude. For example, the energy of a unit type-III wave is higher than that of a unit type-I wave when $\omega < 4.7$. Note that the power flow associated with the type-I wave becomes very large as the wave frequency nears the passband bounding frequency, $\omega = 4.9318$. Since this bounding frequency is very close to the resonant frequency of the diagonal structural members, $\omega = \pi^2/2$, we infer that near the passband edge the deflection pattern of the type-I wave features resonance of diago-

nal structural members (see reference 5 for the corresponding wave shape). For this nearly resonant case the coupling forces at the bay junctions become very large, which leads to the very large power flow observed in Fig. 5 for the type-I wave near its passband edge. A similar pattern of large power flow is observed for the type-II and III waves when the frequency approaches $\omega = \pi^2$, which is the resonant frequency of the longeron structural members.

3.1.2 Wave Propagation In Disordered Truss Beams

Here we use the algorithm developed in Section 2.2 to examine the propagation of characteristic waves in the disordered truss beam. Besides examining wave shapes at various frequencies, we calculate the power flow in an attempt to quantify the strength of localization phenomena. We also examine the magnitude of the various transmitted waves (the modulus of the complex components of $\mathbf{R}_n$) throughout the structure in order to capture the mechanisms of localization and wave conversion. Several representative frequencies are examined below.

At $\omega = 3$

At this frequency, both type-I and -III waves are passband waves. Figure 6 depicts the propagation of a selected type-I wave incident from the left. For the perfectly periodic truss beam the wave features a global bending pattern shown in Fig. 6a. Although Fig. 6b is for a truss beam with a relatively large disorder level of $\sigma = 10\%$, observe that the wave remains unattenuated and nearly identical to that shown in Fig. 6a, even after traveling through 200 disordered bays. This result is consistent with the general observation for mono-coupled systems that waves which featuring global vibration patterns are little subject to localization (although localization eventually takes place if the number of bays keeps increasing).

At $\omega = 4.92$

Figure 7 illustrates a case of severe localization. At frequency $\omega = 4.92$, type-I and -III waves are passband waves. Observe in Figs. 7a and 7c the unattenuated propagation of these two waves along the ordered truss beam. The deflection patterns for both waves feature the local vibrations of the diagonal structural members. For the disordered truss beam the disorder level is $\sigma = 0.3\%$. Comparing Fig. 7c and d, we note that very little localization occurs for the type-III wave in the disordered structure, although the deflection pattern is substantially affected by disorder. Examining Figs. 7a and b, however, we observe the severe localization of the type-I wave to the first few bays of the disordered truss beam. Hence the type-I wave is highly sensitive to small disorder at this frequency. Note that in this case the frequency is very close to the upper passband edge of the type-I wave ($\omega = 4.9318$), hence the strong localization wave observed in Fig. 7b appears consistent with the result for mono-coupled systems that localization is strongest near passband edges.

In order to examine wave interactions in this case, consider a type-I wave of unit amplitude, incident from the left to the same disordered truss beam as in Fig. 7b. The magnitudes of the complex amplitudes of the four transmitted characteristic waves (the modulus of the elements of $\mathbf{R}_n$) are calculated and plotted in Fig. 8 versus the bay number. First note that the magnitude of the type-I incident wave decreases sharply as the bay number increases and rapidly goes to zero, which is consistent with the localization shown in Fig. 7b. Also observe that within the first few bays a small portion of the energy of the incident wave is converted into the type-II and -III waves. Since the type-II wave is a stopband wave, its contribution decays quickly, but note that the converted type-III wave keeps traveling with almost constant amplitude until the end of the disordered segment, which is consistent with the fact that nearly no localization of type-III wave is depicted in Fig. 7d. This is an example of the wave conversion phenomenon that can occur in multi-coupled systems. However, since in this case the converted portion of the incident wave energy is so small, the strong localization of the type-I wave still takes place.

Although the first few bays in Fig. 7b display a substantial deflection, we found that the power flow for the disordered beam is approximately only 0.1% of that associated with the unattenuated type-I wave in the ordered beam. Recall that Eq. (35) shows that the existence of reflected waves ($\mathbf{L}_n$) reduces the power flow along the structure. In order to understand the small value of power flow obtained in the disordered case, we examined the magnitude of the accompanying reflected type-I wave along the beam and found that it nearly coincides with that of the transmitted type-I wave shown in Fig. 8. Physically this means that the transmitted and reflected type-I waves are nearly identical waves but traveling in opposite directions. Hence these two waves almost form a standing wave along the disordered structure (if we neglect the small phase difference between the opposite wave pairs). Since standing waves do not produce power flow, the vibrational energy of the type-I wave is thus confined to a small geometric region with little contribution to the power flow, such that the net power flow in the disordered beam is mainly supported by the type-III wave. On the other hand, the power flow for the case of an incident type-III wave in the disordered beam (see Fig. 7d) is only 2% smaller than that associated with the unattenuated type-III wave in the ordered beam. This confirms that the type-III wave does not localize.

A one-cycle time simulation of the localized type-I wave displayed in Fig. 7b is depicted in Fig. 9 for five successive instants of time. As expected, we observe that the region in which the wave is localized does not travel: the bending component of the wave remains confined near the incidence region. This simulation shows that localized waves do not propagate, which confirms the above explanation regarding power flow.

At $\omega = 19.45$

The above results are for frequencies that are smaller than the fundamental natural frequency of the vertical longeron beam. In order to determine the sensitivity of the wave dynamics to disorder at higher frequencies, we investigate the propagation of waves at $\omega = 19.45$. At this frequency there are two wave pairs in passbands, namely the type-I and -III waves. This frequency is close to the upper bounding frequency ($\omega = 19.576$) of the type-III wave. The results are shown in Fig. 10. Observe that the type-III wave exhibits severe localization for a disorder level $\sigma = 0.2\%$. The type-I wave, although somewhat altered, does not localize. This demonstrates that the dynamics of the truss beam can be sensitive to disorder at high frequencies. It also confirms that localization is strong for frequencies close to a passband edge, and thus that the phase of the incident wave is a key factor in localization.

The results for Case 1 suggest that (1) a wave of a given type can become drastically localized if it leaks only a small portion of its energy to other waves less prone to localization, in which case the system behaves essentially like a mono-coupled one, (2) strong localization takes place when the frequency is close to an edge of the incident wave's passbands, and (3), localization is weak for a wave which features a global vibration pattern at low frequencies (as opposed to a pattern characterized by the local vibration of individual members).

3.2 CASE II: WAVE CONVERSION PHENOMENON

The truss beam examined here is the same as in Case I, except that the axial stiffness of the structural members has been decreased by a factor one hundred, such that $EA = 1.93977 \times 10^5\ N$. This reduced axial rigidity allows for increased interactions between the bending and axial vibrations of the structural members, which in turn favorizes the exchange of energy among the various waves in the disordered case. This makes for richer results regarding localization and wave conversion phenomena. Such interactions were quite weak in Case I (see Fig. 8) because of the high energy

required to excite the very stiff axial motion.

3.2.1 Identification of Characteristic Waves

As in Case I, the characteristic waves of the ordered truss beam are first identified. Figures 11 through 14 depict the propagation constants for the four pairs of characteristic waves as a function of frequency. Recall that the characteristic constant for a wave is defined as the logarithm of the corresponding eigenvalue of the ordered transfer matrix. Each figure displays (1) the real part of the propagation constant, γ, which is the rate of exponential amplitude decay of the wave and (2), the imaginary part of the propagation constant, κ, which is the change in phase from bay to bay. Regions where the exponential decay rate is equal to zero are passbands, in which waves propagate unattenuated. Regions defined by $\gamma > 0$ can be either stopbands or complexbands, corresponding to an attenuated wave. In stopbands the phase change per bay, κ, equals either 0 or π, yielding standing attenuated waves. In complexbands κ is generally different from 0 or π, corresponding to waves that are both traveling and attenuated.

As in Case I, the wave pairs labeled I, II, and III are respectively bending, shear, and compression waves at low frequencies (say $\omega < 4.3$). Figure 14 shows that in most of the frequency range considered ($\omega < 7.96$) the wave pair labeled IV belongs to a stopband and features a very large decay constant. Table 1 lists the frequencies that bound the passbands in the frequency range considered. We find that the bending wave's first passband ranges from $\omega = 0$ to 4.6707. Within this range there are two other wave pairs that feature a passband, namely the bending and compression waves. Other passbands are located as follows: for $4.6707 < \omega < 5.5930$, only type III is in passband; for $5.5930 \leq \omega < 5.8969$, types II and III are in passbands; for $5.8969 \leq \omega \leq 7.9488$, types I, II, and III are in passbands; for $7.9488 < \omega < 7.9688$, types I and II are in passbands; for $7.9688 \leq \omega \leq 9.2272$, types I, II, and IV are in passbands; and for $9.2272 < \omega < \pi^2$; types I and IV are in passbands.

Figure 15 depicts the power flow associated with the four pairs of characteristic waves as a function of frequency. The passband regions displayed in Fig. 15 (those with positive power flow) confirm those found in Figs. 11-14. Observe that contrary to the results shown in Fig. 5 for Case I, the power flow associated with the type-I wave does not become very large as the wave frequency nears the passband bounding frequency $\omega = 4.6707$. We explain this by noting that in the case of smaller axial rigidity, the passband edge is much farther than in Case I from the resonant frequency of the diagonal structural members, $\omega = \pi^2/2$. This leads to less severe vibrations of the diagonal members near the passband edge and thus to smaller coupling forces at the bay junctions, which in turn gives a smaller power flow. On the other hand, the power flow associated with the type-I wave becomes very large near its second passband's upper edge, $\omega = \pi^2$. This is because this bounding frequency is also the resonant frequency of the longerons.

3.2.2 Disordered Truss Beam Dynamics

Wave propagation in the disordered truss beam is studied for several disorder levels and representative frequencies.

At $\omega = 4.2$

At this frequency, both type-I and -III waves belong to passbands. Figure 16 depicts the power flow associated with type-I and type-III waves of unit amplitude incident from the left to the truss beam, as a function of disorder standard deviation. First note that the power flow generally decreases as the disorder increases. This signals the occurrence of localization. However, the power flow associated with the type-I wave increases from approximately $\sigma = 5\%$ to $\sigma = 5.6\%$, after which its decrease is resumed. Also, the power flow of the type-III wave decreases at a much higher rate for $5\% < \sigma < 5.6\%$, after which it experiences a rapid increase. The variation of the power flow shown in Fig. 16 at the higher disorder levels suggests an interaction between the two types of waves. Hence we choose to evidence the wave conversion phenomenon for $\sigma = 5.6\%$ and $\sigma = 6\%$.

First, we select a type-I wave of unit amplitude incident from the left to a disordered beam with $\sigma = 5.6\%$. The magnitudes of the complex amplitudes of the four transmitted characteristic waves are plotted in Fig. 17 versus the bay number. Observe that the magnitude of the type-I wave decreases consistently to reach about 0.4 near the 60th bay, after which it experiences a rapid decrease. However, a large portion of the first wave's energy is converted to the type-III wave, which grows from 0 to about 0.4 within the first 60 bays. Subsequently the type-III wave sustains its motion throughout the entire truss beam and begins decaying slightly only after the 120th bay. Note that the magnitude of the type-III wave is larger than that of the type-I wave over much of the truss beam, *even though the wave incident to the structure is purely of the first type.* When the four transmitted waves leave the disordered segment, the vibration of the truss beam is dominated by both the type-III wave, of magnitude 0.38, and the type-I wave, of magnitude 0.2. Also note the small but consistent contribution of the type-II and -IV waves, which at this frequency belong to stopbands.

Figure 17 evidences the *wave conversion phenomenon* in disordered multi-coupled structures. While the type-I incident wave is subject to strong localization, as attested by its rapid initial decrease in magnitude, it succeeds in leaking its energy to another wave (type III) that is less subject to localization, thereby allowing for sustained motion along the truss beam. The occurrence of wave conversion thus means that localization is more difficult to obtain in multi-coupled than in monocoupled structures, where no wave conversion can take place.

Next, we select a type-III wave of unit amplitude incident to the same disordered beam as in Fig. 17. The magnitudes of the four transmitted waves are shown in Fig. 18 versus the bay number. The magnitude of the type-III wave decreases rapidly and remains approximately at the value 0.2 past the 60th bay. However, observe the massive leakage of energy from the type-III to the type-I wave over the first 70 bays. Here the wave conversion is so great that there is not only no global localization of the motion, but also a doubling of the motion amplitude from that of the incident wave. Once most of the energy has been converted to the type-I wave, though, this wave is subject to localization and decays rapidly. It is interesting to note that the decay pattern for the type-I wave after the 70th bay is quite similar to that featured in Fig. 17. When the four transmitted waves leave the disordered segment, the motion is strongly localized and the truss beam vibration is composed of the type-III wave, of magnitude 0.2, and the type-I wave, of magnitude 0.15.

Figure 19 depicts the magnitudes of the four transmitted waves when a type-I wave of unit-amplitude is incident to a disordered beam with $\sigma = 6\%$. Observe that the type-I wave is subject to severe localization and converts a large portion of its energy to the type-III wave. Again the latter wave is sustained throughout the beam and its magnitude becomes consistently larger than that of the type-I wave. When the four transmitted waves leave the disordered segment, only the type-III and type-I waves have substantial magnitudes of 0.32 and 0.14, respectively. These are smaller than the corresponding magnitudes observed in Fig. 17, which implies that the power flow in Fig. 19 is smaller than that in Fig. 17. This is consistent with the drop in power flow observed in Fig. 16 for the type-I wave as disorder increases from $\sigma = 5.6\%$ to 6%.

Next, Fig. 20 is as Fig. 19 but for a type-III incident wave. The magnitude patterns in Fig. 20 are similar to those displayed in Fig. 18, except that the wave conversion is perhaps not quite as spectacular. Moreover, the magnitudes of the waves that exit the disordered segment are larger in Fig. 20 than in Fig. 18. This again

is consistent with the increase in power flow observed in Fig. 16 for the type-III wave as σ increases from 5.6% to 6%.

The deflection patterns for waves traveling through ordered and disordered truss beams are shown in Figs. 21 and 22. Figures 21a and 22a display the unattenuated propagation of type-I and -III waves in an ordered truss beam, respectively. The type-I wave features a global bending motion, while for the type-III wave the deflection pattern is one of compression. Figure 21b depicts selected portions of the deflection pattern for a type-I wave incident to a disordered truss beam with $\sigma = 6\%$. Observe that the bending character of the motion is rapidly attenuated over the first twenty bays or so, and that a conversion to a compression-type motion takes place. Indeed, over the last thirty bays the deflection pattern of the truss beam is quite similar to that featured in Fig. 22a for the type-III compression wave. Thus the deflection pattern in Fig. 21b agrees well with the wave magnitudes shown in Fig. 19. Also note that the power flow in the disordered case is about 21% of that associated with the unattenuated type-I wave in the ordered beam (see Fig. 16). This indicates that localization, although substantial, is not nearly total because the less localized type-III wave becomes the vehicle for power transmission.

Figure 22b is for a type-III compression wave traveling through the same disordered beam as in Fig. 21b. Observe that a very substantial excitation of the type-I wave takes place approximately from bay 20 to bay 70. This is clearly evidenced by the bending character of the wave, which is similar to that shown in Fig. 21a for an ordered beam. Past bay 70 the converted bending wave decays and its attenuation is remarkably similar to that shown in Fig. 21b for an incident bending wave. In particular, the converted bending wave, while decaying, "re-converts" into a type-III compression wave, as clearly seen over the last thirty bays in Fig. 22b. The deflection pattern depicted in Figs. 22b is thus fully consistent with the wave magnitude variations shown in Fig. 20. Note that the power flow in this disordered case is approximately 28% of that associated with the unattenuated type-III wave in the ordered beam (see Fig. 16). This verifies that type-III wave is not strongly localized for $\sigma = 6\%$.

Figure 23 shows an interesting result. In Fig. 23a a type-II wave, which for $\omega = 4.2$ belongs to a stopband, is incident to a periodic truss beam. Since there is no scattering, the incident wave magnitude decays exponentially. The same wave but incident to a disordered beam with $\sigma = 13.9\%$ is shown in Fig. 23b. We note that the type-II incident wave rapidly converts its energy to both type-I and -III waves. As a result, the wave motion extends much farther into the disordered beam than it does in the ordered system in Fig. 23a. These multiple energy conversions are made possible solely by the reflections and wave interactions at the disordered bay junctions. This result demonstrates that it is possible for a stopband wave to travel significantly farther in a disordered system than in an ordered system, because of the leakage of energy. However, note that we had to select a relatively large disorder to obtain this effect.

At $\omega = 4.62$:

At this frequency, both type-I and -III waves belong to passbands. The unattenuated deflection patterns of these two waves in a periodic beam are depicted in Figs. 24a and 24c, respectively. In Fig. 24d, a type-III wave is incident to a disordered beam for $\sigma = 0.8\%$. We observe that very little, if any, localization occurs. In this case the power flow was found to be 88% of that for the type-III wave in the ordered beam, which confirms that the wave does not become confined.

Figure 24b is for a type-I wave incident to the same disordered beam as in Fig. 24d. Note that the wave becomes localized but not nearly as severely as in Fig. 7b (Case I), although here the frequency is also close to the first bounding frequency of the type-I wave, $\omega = 4.6707$. The wave magnitudes are plotted in Fig. 25 versus the bay number. The type-I wave converts part of its energy into the type-III wave, but since the type-III wave does not localize, its propagation is sustained without much attenuation. In this case the power flow is 5% of that associated with the unattenuated type-I wave in the ordered beam, which confirms the substantial localization.

At $\omega = 5.4$:

At this frequency only the type-III wave belongs to a passband. Figure 26a depicts the unattenuated propagation of this wave in the ordered truss beam. The deflection pattern features a small global bending as well as a local bending of diagonal and horizontal structural members. Although global bending patterns are generally not sensitive to disorder at low frequencies, in Fig. 26b we observe that both global and local vibrations localize. Note that since the type-III wave is the only passband wave at this frequency, it cannot leak its energy to other passband waves to sustain motion propagation.

The above results tell us that a wave of a given type can become localized and then leak its energy to other waves less prone to localization in order to sustain motion propagation. This wave conversion phenomenon can only occur in multi-coupled structures and appears to weaken the degree of localization of incident waves. Power flow is a useful descriptor of both localization and wave conversion phenomena.

4. LOCALIZATION OF NORMAL MODES IN A FIXED-FIXED TRUSS BEAM

Here, we use the formulation of Section 2.4 to investigate the localization of the normal modes of a fixed-fixed, 40-bay disordered truss beam with a disorder level $\sigma = 4.0\%$. All other parameters are the same as for Case II in Section 3.2. Before discussing the localization of mode shapes, we first obtain the normal modes of the associated ordered truss beam and compare them to those in Chen and Pierre,[5] where a higher axial rigidity was used.

We find 51 normal modes in the frequency range $\omega \in [0, 4.6707]$ (*i.e.*, the first passband of the bending wave). Chen and Pierre[5] obtained 40 normal modes in the first passband of the bending wave. Thus, even though in the present study the passband is narrower, we obtain 11 additional normal modes. This can be explained as follows. In Chen and Pierre,[5] the axial rigidity was much larger than the bending rigidity, hence the 40 modes resulted primarily from the bending of the structural members. In the present case, however, the smaller axial rigidity enhances the presence of axial vibrations in the modes, especially since compression waves also propagate in this frequency range. This explains the 11 additional normal modes in the first passband.

These 51 normal modes feature a bending vibration pattern or one of compression, or the combination of the two. Figure 27 displays typical examples of these three types of modes. The transition from a global to a local vibration pattern occurs near $\omega = 4.3$, that is, at a higher frequency than for the truss beam studied in Chen and Pierre.[5]

We obtain a total of 172 normal modes for the periodic truss beam in the frequency range $[0, \pi^2]$. In the same frequency range we find 170 normal modes for the disordered truss beam with $\sigma = 4.0\%$. This means that two modes shift out of the frequency range due to disorder. Figure 28 depicts the modal distribution in the frequency range $[0, \pi^2]$. We observe that the modal density becomes very high for the higher frequency range. The modal density is also high near the passband edges given in Table 1.

Figure 28 also displays the effects of disorder on the natural frequencies. We observe that the change in the natural frequencies due to disorder is more pronounced in the higher modes. This suggests that the dynamics of the truss beam is more sensitive to disorder at high frequencies, as was observed in Section 3.

Figures 29 through 31 display selected normal modes of ordered and disordered ($\sigma = 4\%$) truss beams. Figure 29 displays the

first mode shapes of ordered and disordered beams. Observe the very low natural frequencies of these modes. Also observe that both modes feature the same global bending pattern and that no localization occurs. Figure 30 is for the 46th normal mode, which features primarily motion of the diagonal structural members. The severe localization of that mode to a small region of the truss beam is shown. In Fig. 31 the localization of the 169th normal mode is shown. The ordered mode features primarily local vibrations of the longeron beams and it undergoes severe localization in the disordered case.

These results suggest that (1) the localization phenomenon does not seem to occur for mode shapes that feature global vibration patterns (as opposed to patterns where individual members resonate) and (2), the leakage of energy from one wave-type to another, which was observed in the wave propagation problem, is not obvious to identify for the normal modes.

5. CONCLUSIONS

We have tackled the difficult problem of localization in a nearly periodic, multi-coupled truss beam. We have examined the effects of small random disorder on both the propagation of waves in infinite structures and the normal modes of vibration of finite truss beams. The primary findings are as follows.

The localization phenomenon in disordered multi-coupled structures exhibits a complicated wave interaction mechanism, which we refer to as the *wave conversion phenomenon*. An incident wave that is subject to localization can transfer energy to another wave which is less prone to localization, thereby sustaining the transmission of vibration along the structure and lessening the confinement effect of disorder. This leakage of energy to another wave is probably characteristic of localization in disordered multi-coupled structures, which has never been studied formally in structural dynamics. It suggests that localization is more difficult to obtain in multi-coupled than in mono-coupled structures, much in the same way as localization is easier to produce in one-dimensional systems than in two- or three-dimensional ones.

A non-propagating wave that belongs to the stopband of an ordered structure can, in a disordered structure, leak its energy to other waves that are only weakly subject to localization. Thus, a stopband wave in a disordered truss beam can induce a long-range propagation that would not take place in the ordered structure.

Small random disorder in a truss beam also causes the localization of the normal modes of vibration to small geometric regions. We found that mode localization occurs primarily at higher frequencies, that is, when individual structural members resonate. It does not occur for the very-low-frequency global vibration modes.

REFERENCES

1. Pierre, C., "Weak and Strong Vibration Localization in Disordered Structures: A Statistical Investigation," *Journal of Sound and Vibration*, Vol. 139, No. 1, 1990, pp. 111-132.
2. Hodges, C. H., "Confinement of Vibration by Structural Irregularity," *Journal of Sound and Vibration*, Vol. 82, No. 3, 1982, pp. 411-424.
3. Bendiksen, O. O., "Mode Localization Phenomena in Large Space Structures," *AIAA Journal*, Vol. 25, No. 9, 1987, pp. 1241-1248.
4. Kissel, G. J., "Localization in Disordered Periodic Structures," Ph.D. *Dissertation, Massachusetts Institute of Technology*, 1988.
5. Chen, W. J., and Pierre, C., "Exact Linear Dynamics of a Periodic Truss Beam: Normal Modes of Vibration and Harmonic Wave Propagation," *32nd AIAA/ASME/ASCE/AHS/ASC Structures, Structural Dynamics, and Materials Conference*, 1991.
6. Friedmann, P., Lust, S., and Bendiksen, O., "Free and Forced Response of Nearly Periodic Multi-Span Beams and Multi-Bay Trusses," *32nd AIAA/ASME/ASCE/AHS/ASC Structures, Structural Dynamics, and Materials Conference*, 1991.
7. Igusa, T., and Tang, Y., "Mobilities of Periodic Structures in Terms of Asymptotic Modal Properties," *32nd AIAA/ASME /ASCE/AHS/ASC Structures, Structural Dynamics, and Materials Conference*, 1991.
8. Noble, B., and Daniel, J. W., *Applied Linear Algebra*, Second Edition, 1977, Prentice-Hall, Inc., New Jersey.
9. Mead, D. J., "A General Theory of Harmonic Wave Propagation in Linear Periodic Systems with Multiple Coupling," *Journal of Sound and Vibration*, Vol. 27, 1973, pp. 235-260.
10. Signorelli, J., and von Flotow, A. H., "Wave Propagation, Power Flow, and Resonance in a Truss Beam," *Journal of Sound and Vibration*, Vol. 126, 1988, pp. 127-144.

APPENDIX A: POWER FLOW IN PERIODIC STRUCTURES

Here we use Eqs. (28) and (34) to show that in an undamped periodic structure the power flow associated with a passband wave is positive and constant along the structure, while complexband or stopband waves do not transmit power. Consider a wave incident from the left to a perfectly periodic structure. Its amplitude is multiplied by $1/\lambda$ at each bay, where λ is the eigenvalue of the transfer matrix $\mathbf{T}_o$ associated with the corresponding left-traveling wave.[5] Hence the incident wave is governed by $\mathbf{u}_{n+1} = \frac{1}{\lambda}\mathbf{u}_n$.

(1) For frequencies in the stopband: Then λ is real, with $|\lambda| > 1$. Since all displacement vectors $\mathbf{u}_n$ are real, we obtain

$$P_n = -\frac{\omega}{2}\mathrm{Im}[\mathbf{u}_{n+1}^{*T}\mathbf{C}\mathbf{u}_n] = 0 \qquad (A1)$$

where the matrix $\mathbf{C}_n$ in Eq. (28) can be denoted by $\mathbf{C}$ for a periodic structure.

(2) For frequencies in the passband: Here $\lambda = e^{\pm j\kappa}$, with $\kappa \in (0, \pi)$. This leads to

$$P_{n+1} = -\frac{\omega}{2}\mathrm{Im}[\mathbf{u}_{n+2}^{*T}\mathbf{C}\mathbf{u}_{n+1}] \qquad (A2)$$

$$= -\frac{\omega}{2}\mathrm{Im}[e^{\pm j\kappa}\mathbf{u}_{n+1}^{*T}\mathbf{C}e^{\mp j\kappa}\mathbf{u}_n] \qquad (A3)$$

$$= -\frac{\omega}{2}\mathrm{Im}[\mathbf{u}_{n+1}^{*T}\mathbf{C}\mathbf{u}_n] = P_n \qquad (A4)$$

(3) For the passband bounding frequencies: Then $\lambda = \pm 1$, which yields a non-attenuating wave with adjacent bays vibrating in or out of phase, *i.e.*, a standing wave. Since all the displacement vectors are real, from case (1) the power flow is zero.

(4) For frequencies in the complexband: Then $\lambda = e^{\gamma \pm j\kappa}$, with $\gamma > 0$ and $\kappa \in (0, \pi)$. Here we use Eq. (34) to show that the power flow is zero (although it is not strictly necessary). From $\mathbf{u}_{n+1} = \frac{1}{\lambda}\mathbf{u}_n$, we rewrite Eq. (A2) as:

$$\begin{aligned} P_{n+1} &= -\frac{\omega}{2}\mathrm{Im}[e^{-\gamma \pm j\kappa}\mathbf{u}_{n+1}^{*T}\mathbf{C}e^{-\gamma \mp j\kappa}\mathbf{u}_n] \\ &= -e^{-2\gamma}\frac{\omega}{2}\mathrm{Im}[\mathbf{u}_{n+1}^{*T}\mathbf{C}\mathbf{u}_n] \\ &= e^{-2\gamma}P_n \end{aligned} \qquad (A5)$$

Equation (34) states that the power flow associated with undamped periodic or disordered structures is constant, *i.e.*, $P_{n+1} = P_n$. Since $\gamma \neq 0$, the only solution for Eq. (A5) is $P_{n+1} = P_n = 0$

$\lambda = 1$	$\lambda = -1$
5.5930 (II)	4.6707 (I)
5.8969 (I)	7.9488 (III)
7.9688 (IV)	9.2272 (II)
	π^2 (I, II)

Table 1 The dimensionless bounding frequencies of the pass-bands. These correspond to the double eigenvalues $\lambda = 1$ or -1. The parenthetical Roman numerals denote the type of the associated characteristic wave.

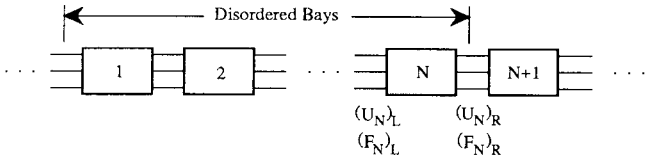

Figure 1 A generic, multi-coupled, nearly periodic structure. Bays 1 through N are disordered bays embedded in an otherwise perfectly periodic and infinite structure.

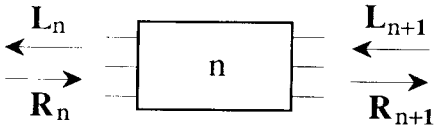

Figure 2 Wave coordinates for an arbitrary nth bay. $\mathbf{L_n}$ contains the m amplitudes of the left-going waves and $\mathbf{R_n}$ the m amplitudes of the right-going waves. The waves entering the nth bay are $\mathbf{R}_n$ and $\mathbf{L}_{n+1}$, and those leaving the bay are $\mathbf{R}_{n+1}$ and $\mathbf{L}_n$.

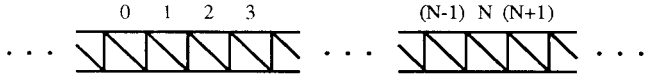

Figure 3 Truss beam assembly connected by pin joints. Bays 1 through N are disordered bays embedded in an otherwise periodic and infinite truss beam.

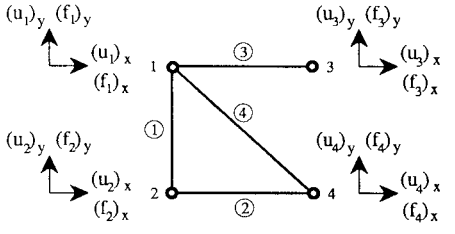

Figure 4 A single bay of the truss beam, consisting of four uniform members with identical material properties.

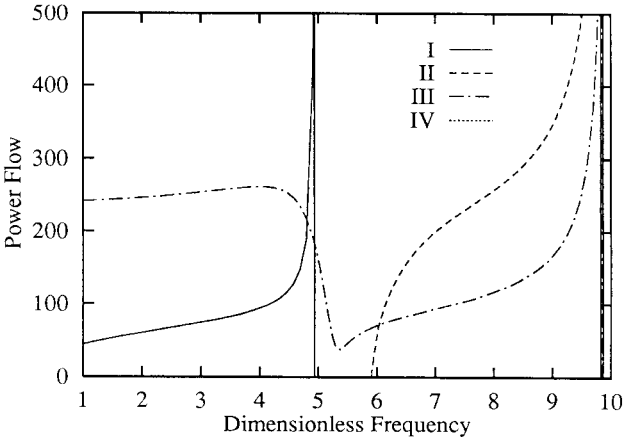

Figure 5 Power flow associated with each of the characteristic waves as a function of frequency. Curve I is for the type-I (bending) wave, curve II for the type-II (shear) wave, and curve III for the type-III (compression) wave. Power flow for the type-IV (evanescent) wave is zero over the range shown.

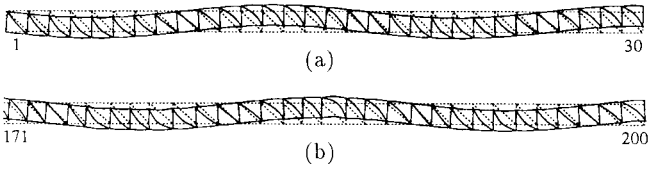

Figure 6 (a) A type-I (bending) wave with frequency $\omega = 3$ travels through a perfectly periodic truss beam. (b) The same wave travels through the last 30 bays of a 200-disordered bay segment. The standard deviation of disorder is $\sigma = 10\%$.

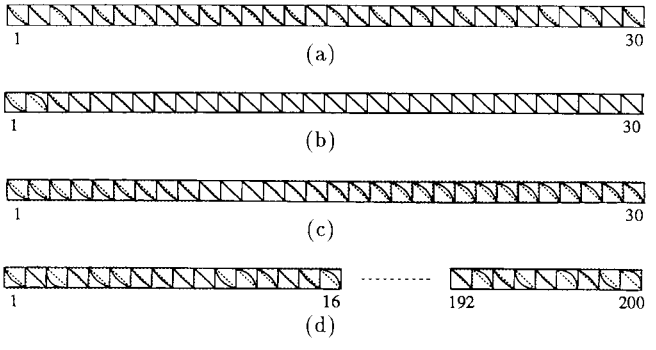

Figure 7 (a) A type-I wave with frequency $\omega = 4.92$ travels through a perfectly periodic truss beam. (b) The same wave travels through the first 30 bays of a 200-disordered bay segment. The standard deviation of disorder is $\sigma = 0.3\%$. (c) A type-III wave with frequency $\omega = 4.92$ travels through an ordered truss beam. (d) The same type-III wave travels through the disordered beam of (b). Selected deflection patterns are shown.

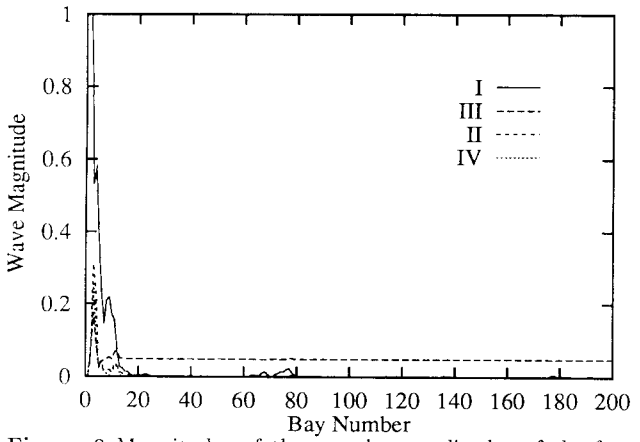

Figure 8 Magnitudes of the complex amplitudes of the four transmitted characteristic waves versus bay number, for a type-I wave of unit amplitude incident to 200 disordered bays. The frequency is $\omega = 4.92$ and the disorder level is $\sigma = 0.3\%$. Curve i is for type-i wave, where i =I, II, III, and IV.

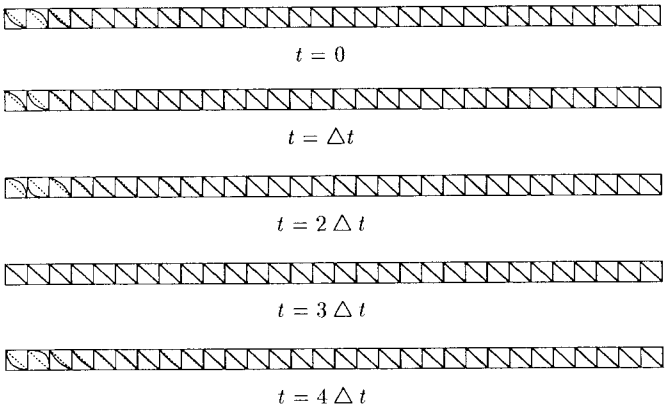

Figure 9 A one-cycle time simulation of the localized type-I wave displayed in Fig. 7b is depicted for five successive instants of time. Deflection patterns are shown at equal time increments of $2\pi/(5\omega)$, where $\omega = 4.92$.

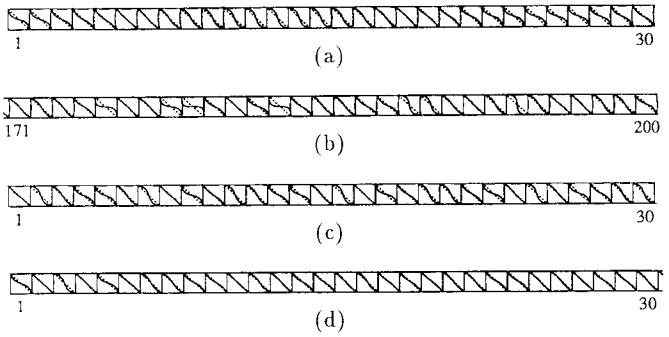

Figure 10 (a) A type-I wave with frequency $\omega = 19.45$ travels through a perfectly periodic truss beam. (b) The same wave travels through the last 30 bays of a 200-disordered bay segment. The disorder is $\sigma = 0.2\%$. (c) A type-III wave with frequency $\omega = 19.45$ travels through a perfectly periodic truss beam. (d) The same type-III wave travels through the first 30 bays of the disordered beam of (b).

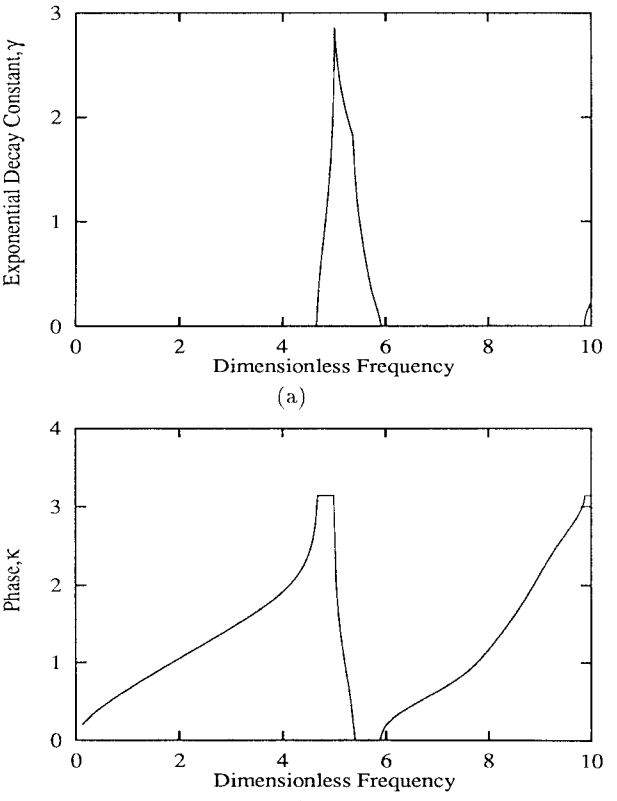

Figure 11 Propagation constant versus frequency for type-I (bending) waves, (a) exponential decay constant, and (b) phase change per bay. Stopbands and complex bands are regions where $\gamma > 0$. Passbands are regions where $\gamma = 0$. The modes of the finite truss beam occur at frequencies which belong to the passbands.

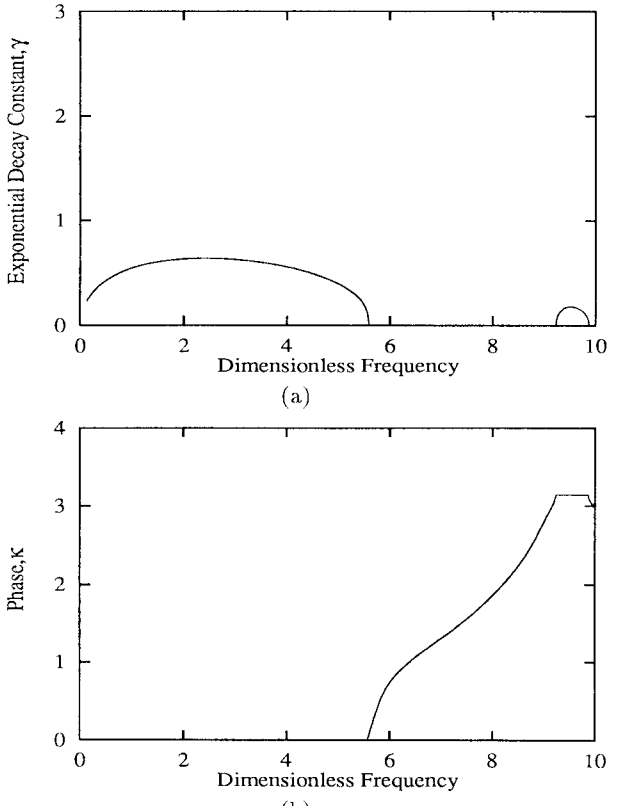

Figure 12 Propagation constant versus frequency for type-II (shear) waves, (a) exponential decay constant, and (b) phase.

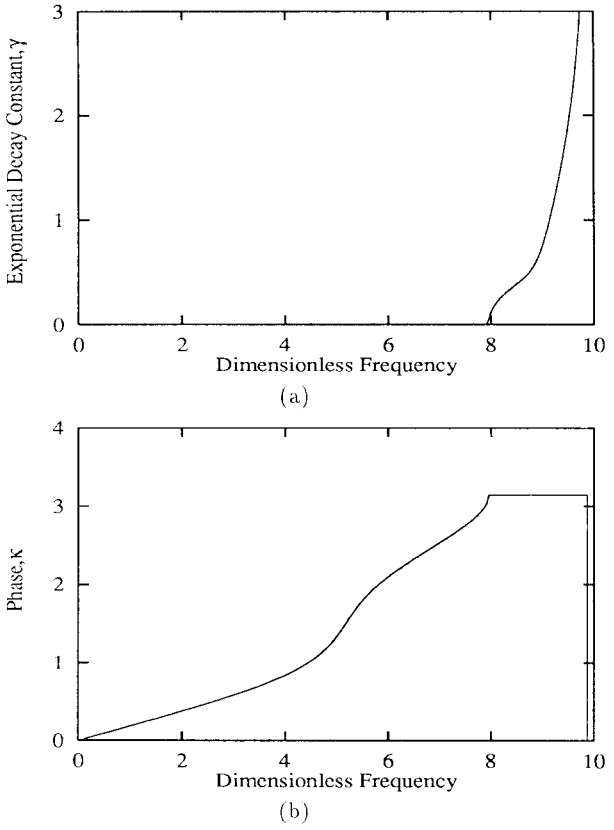

Figure 13 Propagation constant versus frequency for type-III (compression) waves, (a) exponential decay constant, and (b) phase.

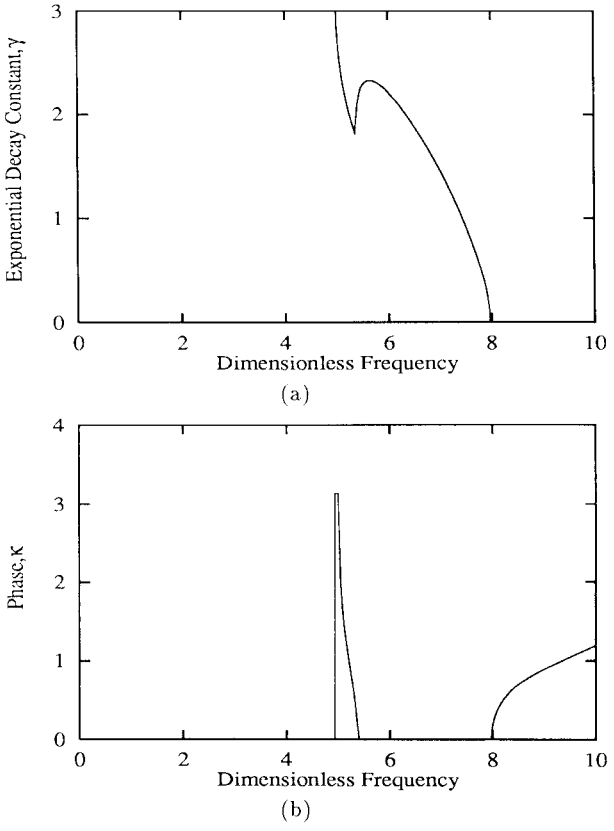

Figure 14 Propagation constant versus frequency for type-IV (evanescent) waves, (a) exponential decay constant, and (b) phase.

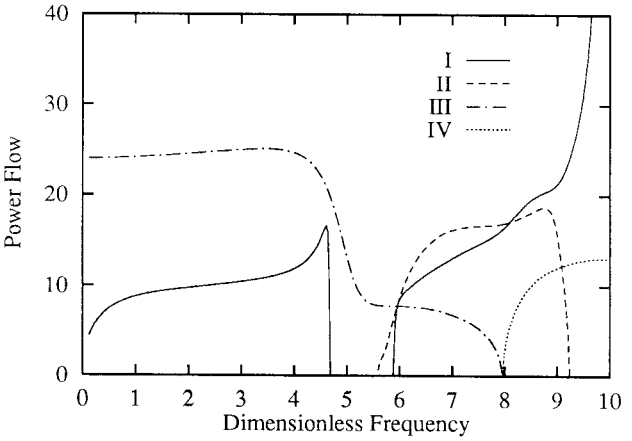

Figure 15 Power flow associated with each of the characteristic waves as a function of frequency. Curve I is for the type-I (bending) wave, curve II for the type-II (shear) wave, curve III for the type-III (compression) wave, and Curve IV for the type-IV (evanescent) wave.

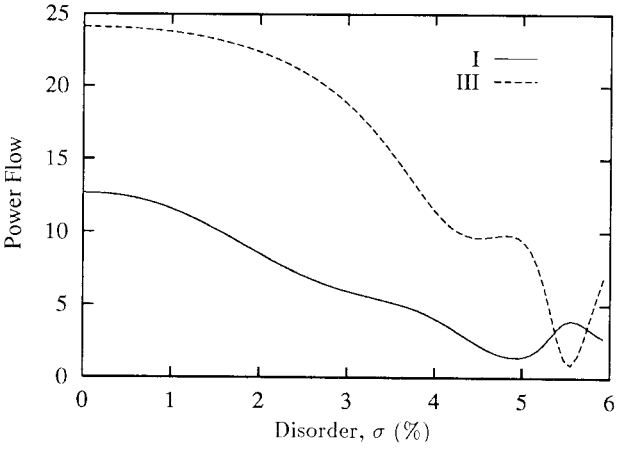

Figure 16 Power flow versus disorder standard deviation for type-I and -III waves incident to 200 disordered bays. The frequency is $\omega = 4.2$

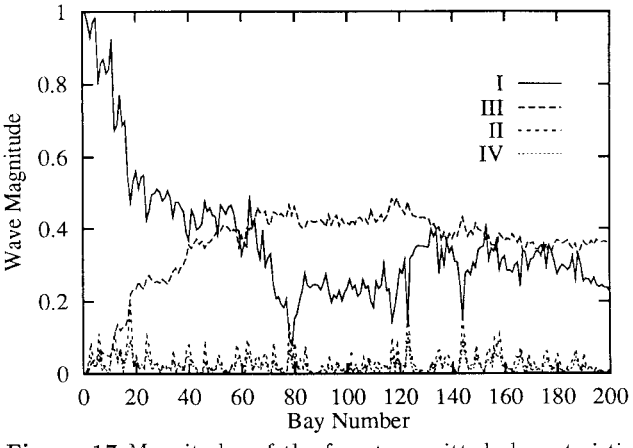

Figure 17 Magnitudes of the four transmitted characteristic waves versus bay number, for a type-I wave of unit amplitude incident to 200 disordered bays. The frequency is $\omega = 4.2$ and the standard deviation of disorder is $\sigma = 5.6\%$. Curve i is for type-i wave, where i=I, II, III, and IV.

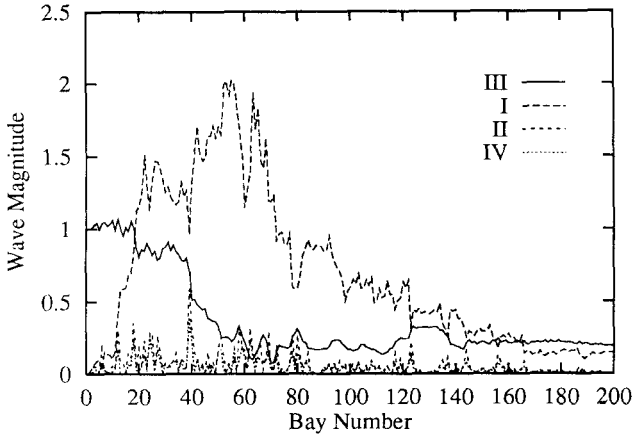

Figure 18 Magnitudes of the four transmitted characteristic waves versus bay number, for a type-III wave of unit amplitude incident to the same disordered truss beam as in Fig. 17. The frequency is $\omega = 4.2$.

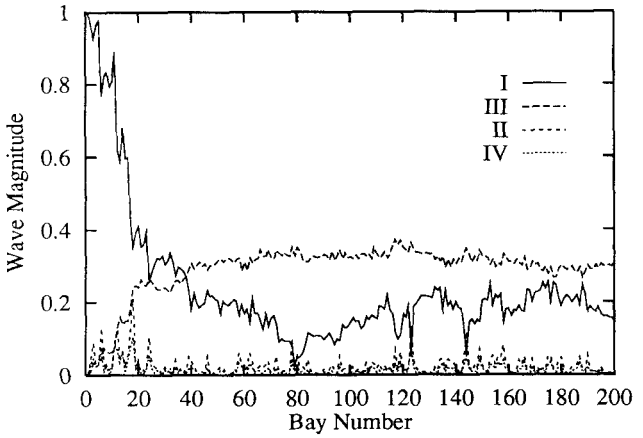

Figure 19 Magnitudes of the four transmitted characteristic waves versus bay number, for a type-I wave of unit amplitude incident to 200 disordered bays. The standard deviation of disorder is $\sigma = 6\%$ and the frequency is $\omega = 4.2$.

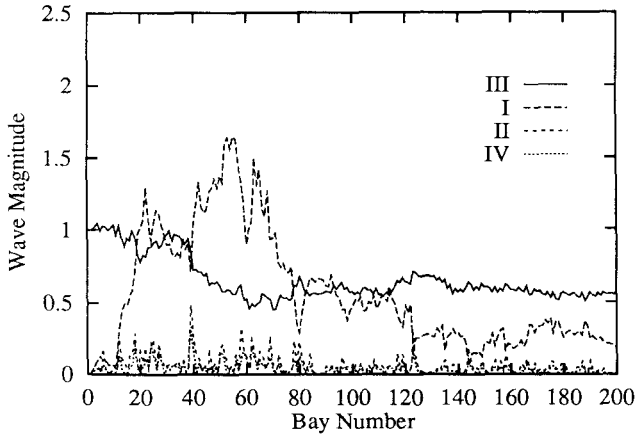

Figure 20 Magnitudes of the four transmitted characteristic waves versus bay number, for a type-III wave of unit amplitude incident to the same disordered truss beam as in Fig. 19. The frequency is $\omega = 4.2$.

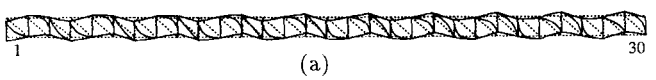

Figure 21

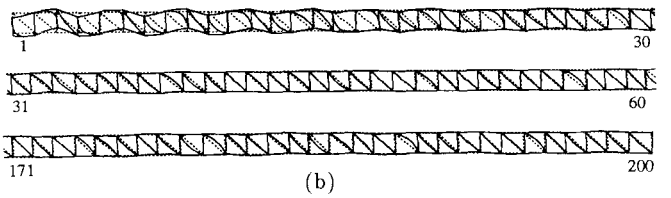

Figure 21 (a) A type-I wave with frequency $\omega = 4.2$ travels through a perfectly periodic truss beam. (b) The same wave travels through a 200-disordered bay segment. The standard deviation of disorder is $\sigma = 6\%$. Selected portions of the deflection patterns are shown.

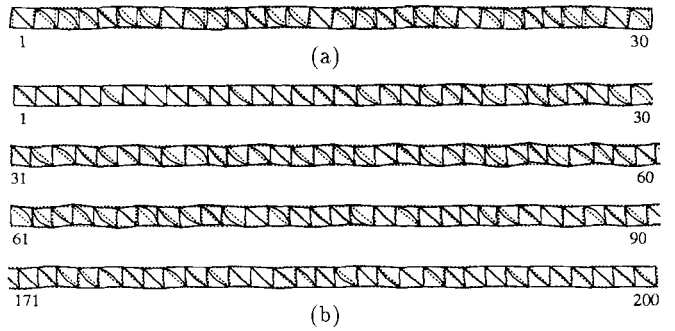

Figure 22 (a) A type-III wave with frequency $\omega = 4.2$ travels through a perfectly periodic truss beam. (b) The same wave travels through a 200-disordered bay segment. The disorder is $\sigma = 6\%$. Selected portions of the deflection patterns are shown.

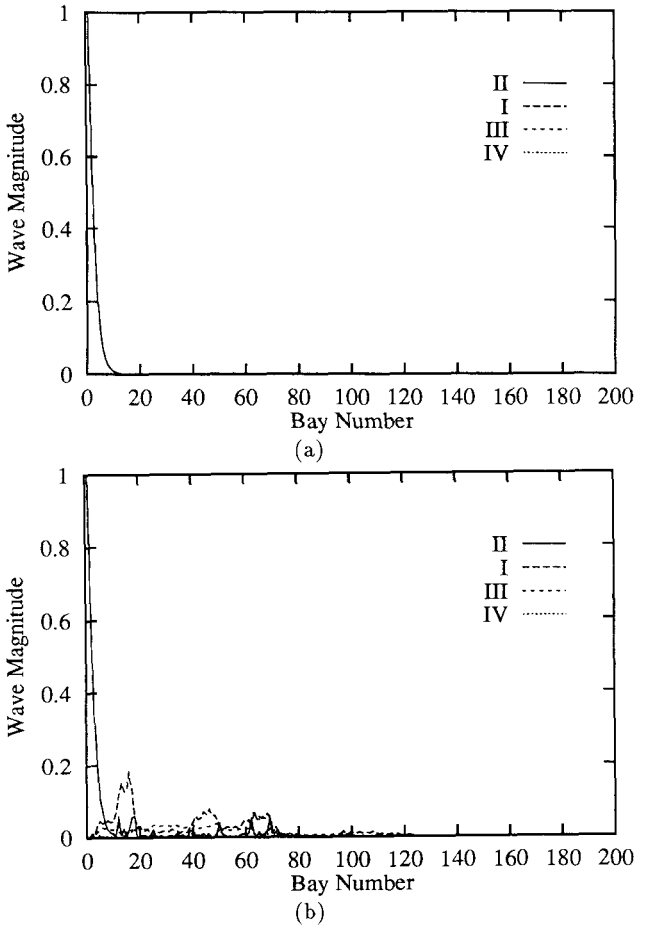

Figure 23 (a) Magnitude of the type-II transmitted wave versus bay number. A unit type-II wave is incident to an ordered truss beam for $\omega = 4.2$. (b) Magnitudes of the four transmitted characteristic waves versus bay number, for the same type-II wave incident to a disordered truss beam with $\sigma = 13.9\%$.

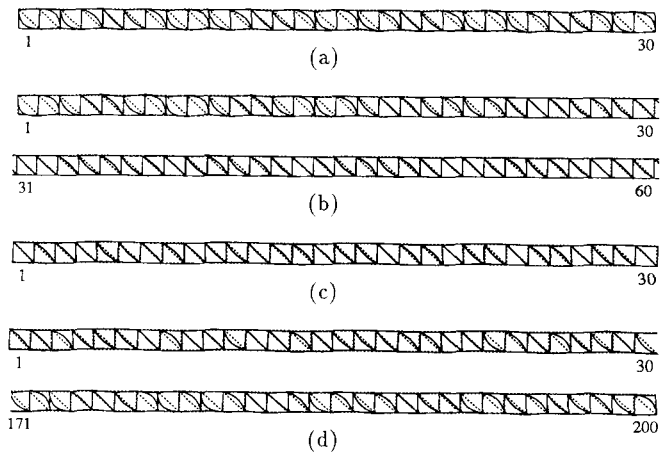

Figure 24 (a) A type-I wave with frequency $\omega = 4.62$ travels through a perfectly periodic truss beam. (b) The same wave travels through a 200-disordered bay segment with $\sigma = 0.8\%$. Selected portions of the wave shape are shown. (c) A type-III wave with frequency $\omega = 4.62$ travels through a perfectly periodic truss beam. (d) The same type-III wave travels through a 200-disordered bay segment with $\sigma = 0.8\%$. Selected bays are shown.

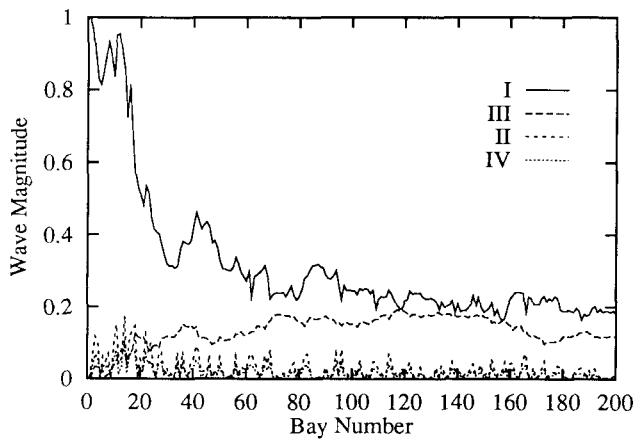

Figure 25 Magnitudes of the four transmitted characteristic waves versus bay number, for a type-I wave of unit amplitude incident to 200 disordered bays. Here, $\omega = 4.62$ and the disorder level is $\sigma = 0.8\%$.

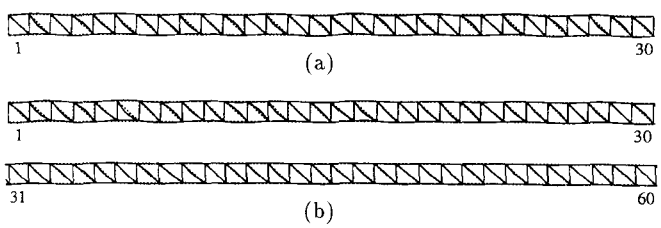

Figure 26 (a) A type-III wave with frequency $\omega = 5.4$ travels through an ordered truss beam. (b) The same wave travels through a 200-disordered bay segment with $\sigma = 5\%$. Selected bays are shown.

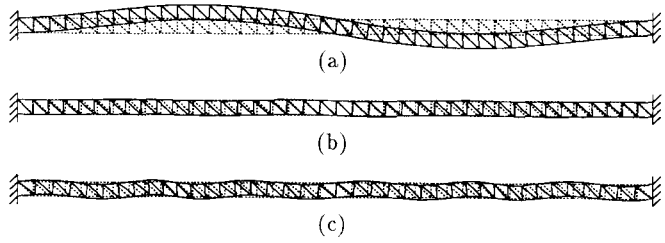

Figure 27 Three global mode shapes for a fixed-fixed periodic truss beam with 40 bays: (a) The 2nd mode, for $\omega = 0.112$, features a pure bending pattern, (b) the 9th mode, for $\omega = 0.8566$, features a pure compression pattern and (c), the 15th mode, for $\omega = 1.6917$, features a mixed bending-compression pattern.

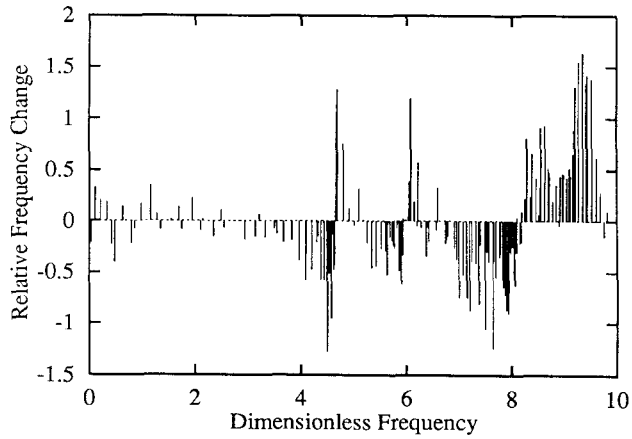

Figure 28 Relative change of the natural frequencies of a 40-bay truss beam due to disorder of standard deviation 4%, versus the natural frequencies of the ordered beam. Each vertical line corresponds to a normal mode of the truss beam. The closeness of the vertical lines also indicates the modal density in a particular frequency range.

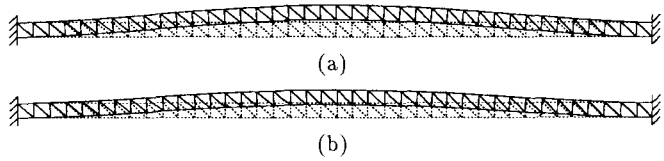

Figure 29 (a) The first mode shape of a 40-bay, ordered, fixed-fixed truss beam. The mode's frequency is $\omega = 0.04056$. (b) The corresponding normal mode of the disordered truss beam with $\sigma = 4\%$. The frequency of this mode is $\omega = 0.04047$.

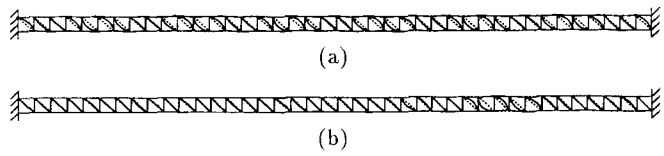

Figure 30 (a) The 46th mode shape of the ordered truss beam in Fig. 29. The mode's frequency is $\omega = 4.597$. (b) The corresponding 46th normal mode of the disordered truss beam with $\sigma = 4\%$. The mode's frequency is $\omega = 4.592$.

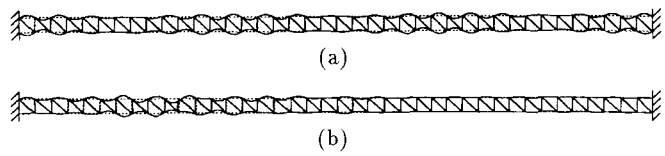

Figure 31 (a) The 169th mode shape of the ordered truss beam in Fig. 29. The mode's frequency is $\omega = 9.76$. (b) The corresponding 169th normal mode of the disordered truss beam with $\sigma = 4\%$. The mode's frequency is $\omega = 9.746$.